

© 2017

Nicole Couto

ALL RIGHTS RESERVED

CIRCULATION AND HEAT TRANSPORT ON THE WEST ANTARCTIC PENINSULA
CONTINENTAL SHELF

By

NICOLE COUTO

A dissertation submitted to the

School of Graduate Studies

Rutgers, The State University of New Jersey

In partial fulfillment of the requirements

For the degree of

Doctor of Philosophy

Graduate Program in Oceanography

Written under the direction of

Oscar Schofield

And approved by

New Brunswick, New Jersey

October, 2017

ABSTRACT OF THE DISSERTATION

Circulation and Heat Transport on the West Antarctic Peninsula Continental Shelf

by NICOLE COUTO

Dissertation Director:

Oscar Schofield

The West Antarctic Peninsula (WAP) has experienced rapid warming over the past several decades, which has resulted in the melting of glaciers and sea ice and created serious consequences for many ice-dependent species. Upper Circumpolar Deep Water (UCDW) is a warm, nutrient-rich water mass found in deep waters off the WAP continental shelf. It is the major source of oceanic heat and nutrients to the shelf waters. This dissertation focuses on the transport of this water mass onto the shelf and its transformation as it moves toward coastal canyons. Data from glider transects along the WAP shelf showed that a significant portion of heat advected onto the shelf is carried in mesoscale eddies. Most of these eddies move across the shelf along the northeastern walls of shelf-incising troughs that open at the shelf break. These mesoscale features steadily lose heat with increasing distance along their paths and may be responsible for as much as 50% of the heat flux onto the shelf. Once on the shelf, UCDW follows complicated pathways toward the coast. Virtual drifters released at several depths near the shelf break in a high-resolution numerical model of the WAP showed that UCDW moves northward along the shelf

slope until it is pulled into the shelf interior at one of several troughs. Drifters were often caught in trough-contained cyclonic gyres, moving shoreward along their northern walls and seaward along their southern walls. They entered Palmer Deep, an ecologically important coastal canyon in the northern part of the WAP, primarily from the northeast. Those that traveled the farthest north before entering the canyon cooled most significantly. Results from the model, along with data from a subsurface mooring deployed at the head of a coastal canyon, were used to describe the nearshore circulation at the end of the UCDW transit. Transport was dominated by a southeastward-flowing current during winter and shifted toward the southwest during summer after sea ice had retreated and when northerly wind intensity was strong. More UCDW entered the canyon during winter than summer, which may be the result of a more barotropic flow during winter that more readily follows bathymetric contours. As wind intensity on the WAP increases and sea ice decreases, the amount of ocean heat reaching ice-dependent coastal ecosystems is likely to increase. The results presented here reveal the complexity of circulation on the WAP and the importance of mesoscale observations in understanding these changes.

Acknowledgements

Thank you to my advisors and committee members, Oscar Schofield, Josh Kohut, Bob Chant, and Doug Martinson. You have all been so supportive at every step of this process. Thank you for always keeping your doors open and offering advice and guidance while still allowing me to create and follow my own path. Doug, thank you for the days spent in your office, working through problem after problem, and for all those freshly made cookies, straight from the package.

Darren McKee and Richard Iannuzzi were incredibly helpful during those days spent at Lamont. Thank you both for being available to bounce ideas around and thanks to Rich for teaching me about mooring design.

So many PIs, postdocs, and graduate students in the Palmer LTER program have become collaborators and friends. Thank you all for sharing your expertise. I am especially grateful to Sharon Stammerjohn who first introduced me to the program in 2010 and was an unbeatable mentor as I took my first steps toward becoming a scientist.

Thank you to Mike Dinniman and Jenny Graham for teaching me about your WAP regional model and for running the drifter experiments for me. You have both been so generous with your time and knowledge.

Thanks to Eli Hunter for responding “yes, how about now?” every time I came by to ask if and when he might be available to help me work my mind around some new mathematical concept.

Thank you to everyone who made field operations run smoothly. Dave Aragon, Tina Haskins, and Chip Haldeman were always wonderful to work with during glider deployments, recoveries, maintenance, and troubleshooting. Thanks also to Chip who helped me build my mooring. Thanks to Teledyne RDI for offering me their Academic Grant award in 2014, which afforded me the opportunity to design the third chapter of this dissertation from scratch. Paul Devine and Debbie King were helpful from start to finish, getting all the equipment to and from the field and making sure the data quality was the best it could be. Thanks to the dozens of support staff at Palmer Station and crew of the R/V *Laurence M. Gould* who made all our operations possible and worked tirelessly to make sure things always went smoothly.

Six years of graduate school are not just about the science. I am so grateful for the friends I made here in New Jersey and the friends and family cheering me on from across the country. I was lucky enough to enter this program with an exceptional cohort who became great friends along with many others in the Oceanography and Ecology programs. Jack, Nicole, Filipa, Christien, Alex, Brittany, Talia, Mikaela, Jackie, Michael, Jennifer, and Chris, thanks for making these years really fun, and for sticking with me through all the ups and downs.

Mom, thank you for hiding your fears whenever I told you I'd be heading out to some of the harshest areas of the ocean. And thank you for showing me by example that women don't have to choose between motherhood and cutting-edge science. Dad, thank you for always sharing your curiosity about the universe with

me, and for helping me cultivate my own curiosity. I couldn't have asked for a better pair of people to guide me through this world. Thanks for everything.

Table of Contents

| | |
|--|-----------|
| Abstract of the Dissertation..... | ii |
| Acknowledgements | iv |
| 1 Introduction..... | 1 |
| 2 Distribution of Upper Circumpolar Deep Water on the continental shelf of the West Antarctic Peninsula | 5 |
| 2.1 Abstract..... | 5 |
| 2.2 Introduction..... | 6 |
| 2.3 Methods..... | 10 |
| 2.4 Results and Discussion..... | 15 |
| 2.4.1 Locations of UCDW intrusions..... | 15 |
| 2.4.2 Properties of UCDW eddies..... | 18 |
| 2.4.3 Heat balance on the WAP..... | 21 |
| 2.5 Conclusions..... | 26 |
| 3 Pathways and retention times in a biologically productive canyon system on the West Antarctic Peninsula | 28 |
| 3.1 Abstract..... | 28 |
| 3.2 Introduction..... | 29 |
| 3.3 Model Description | 33 |
| 3.4 Results | 36 |
| 3.4.1 Pathways from the shelf break to Palmer Deep..... | 36 |
| 3.4.2 Modification of water properties..... | 41 |

| | | |
|------------|--|-----------|
| 3.4.3 | Canyon entry and exit..... | 42 |
| 3.4.4 | Retention time in Palmer Deep..... | 44 |
| 3.5 | Discussion..... | 46 |
| 3.5.1 | Entry onto the WAP shelf..... | 46 |
| 3.5.2 | Interaction with the Antarctic Coastal Current | 48 |
| 3.5.3 | Factors controlling retention time in Palmer Deep | 48 |
| 3.5.4 | Impact of increased model resolution..... | 50 |
| 3.6 | Conclusions | 51 |
| 4 | Tidal and wind-driven controls on heat flux at the head of Palmer Deep Canyon..... | 53 |
| 4.1 | Introduction..... | 53 |
| 4.2 | Background on regional circulation..... | 56 |
| 4.3 | Observations..... | 60 |
| 4.3.1 | Acoustic Doppler Current Profiler (ADCP) and Conductivity-Temperature-Depth (CTD) data | 60 |
| 4.3.2 | Wind | 62 |
| 4.3.3 | Sea ice | 62 |
| 4.4 | Results | 62 |
| 4.4.1 | Seasonal and physical context | 62 |
| 4.4.2 | Currents and heat flux | 64 |
| 4.4.3 | Power spectral density estimates..... | 71 |
| 4.4.4 | Coherence | 74 |
| 4.5 | Discussion..... | 78 |
| 4.5.1 | Influence of the Antarctic Peninsula Coastal Current and winds on local circulation | 78 |

| | | |
|-------|--------------------------------------|-----------|
| 4.5.2 | Local tidal fluctuations | 81 |
| 4.6 | Conclusions | 82 |
| 5 | Summary and Conclusions | 84 |

List of Tables

| | |
|--|----|
| Table 2-1: Coefficients and variables used for heat budget calculations..... | 23 |
| Table 3-1: Timing and locations of drifter releases in the model | 35 |

List of Figures

| | |
|--|----|
| Figure 2-1: Map WAP continental shelf and glider tracks..... | 11 |
| Figure 2-2: Example of method used to define eddy width..... | 13 |
| Figure 2-3: Histograms of UCDW detected on the shelf..... | 16 |
| Figure 2-4: Map and characteristics of eddies on the WAP shelf..... | 20 |
| Figure 2-5: Schematic illustrating the components of the heat budget on the WAP continental shelf..... | 22 |
| Figure 3-1: Map of study area and locations of drifter release points..... | 34 |
| Figure 3-2: Percentages of drifters that reached Palmer Deep..... | 37 |
| Figure 3-3: Counts of drifters within 20 x 20 km grid boxes 14 days before each entered the canyon..... | 39 |
| Figure 3-4: Counts of drifters within 20 x 20 km grid boxes 30 days before each entered the canyon..... | 39 |
| Figure 3-5: Examples of drifter approaches to Palmer Deep..... | 40 |
| Figure 3-6: Changes in drifter temperature and salinity..... | 41 |
| Figure 3-7: Canyon entry and exit by depth..... | 43 |
| Figure 3-8: Canyon entry and exit by season..... | 44 |
| Figure 3-9: Retention time in Palmer Deep..... | 45 |
| Figure 4-1 Map of WAP circulation..... | 58 |
| Figure 4-2: Map of mooring location..... | 60 |
| Figure 4-3: Temperature records at Palmer Station and Station E..... | 63 |
| Figure 4-4: Temperature and salinity trends at the mooring site..... | 65 |

| | |
|---|----|
| Figure 4-5: Sea ice concentration, and low-pass filtered wind direction, current direction, and current speed at Station E mooring site. | 66 |
| Figure 4-6: Time series and polar histograms of velocity and heat flux. | 68 |
| Figure 4-7: Time series and polar histograms of low-pass filtered velocity and heat flux. | 69 |
| Figure 4-8: Time series and polar histograms of high-pass filtered velocity and heat flux. | 70 |
| Figure 4-9: Integrated bottom heat flux over duration of mooring deployment. | 71 |
| Figure 4-10: Power spectral densities of wind, bottom temperature, and current velocities..... | 73 |
| Figure 4-11: Coherence and phase lag between wind and bottom velocity..... | 76 |
| Figure 4-12: Coherence and phase lag between wind and bottom temperature..... | 77 |
| Figure 4-13: Coherence and phase lag between bottom velocity and bottom temperature. | 77 |
| Figure 4-14 Schematic of upwelling at the mooring location. | 82 |

1 Introduction

The ice-ocean system of the western Antarctic Peninsula (WAP) continental shelf region has experienced dramatic physical and ecological changes in recent years. This is a region of the world with some of the fastest-warming atmospheric temperatures, particularly in winter when the rate of warming is the highest globally [Turner *et al.*, 2006]. Warm, salty water originating off the continental shelf in the Antarctic Circumpolar Current (ACC) is thought to be an important contributor to the rising heat of the WAP shelf, but the delivery of this water mass onto the shelf and its transport shoreward toward glacier bases and ice shelves is still not well understood. Several mechanisms for exchange across the shelf break have been identified, including topographic steering, Ekman-driven upwelling, and eddy shedding, but the relative importance of each is still unclear [Moffat *et al.*, 2009; Klinck and Dinniman, 2010; Martinson and McKee, 2012]. Pathways of transport on the shelf itself are also poorly understood, as are the transformation processes that affect this warm, deep water.

Because of its relatively deep bathymetry (~500 m average), exchange between subpycnocline waters on and off the shelf occurs more frequently than on other continental shelves. The proximity of the WAP shelf to the ACC is unique to Antarctic shelves [Orsi *et al.*, 1995], and allows the warm water masses contained in this current to be transported more readily to this part of the continental shelf than elsewhere around the continent. Surface layer temperature and salinity on the WAP

are influenced by solar heating and the growth and melt of sea ice, but below the permanent pycnocline, which is between 100 and 200 m, the deep shelf waters are oceanic in origin. Upper Circumpolar Deep Water (UCDW) is the warm, deep water mass that most readily enters onto the shelf due to its depth in the water column. It is the lighter of two subspecies of the Circumpolar Deep Water, which is the most voluminous water mass in the ACC. Since the 1970s, the core of Circumpolar Deep Water in the ACC has warmed and shoaled [*Schmidtke et al., 2014*]. Over the same period, temperatures on the WAP shelf have risen and been implicated as the primary cause of the growing loss of ice shelves [*Pritchard et al., 2012; Rignot et al., 2013; Cook et al., 2016*].

In addition to its significant effect on the warming of the atmosphere and cryosphere, UCDW is thought to be very important in supporting nearshore biological “hotspots” by supplying heat and nutrients [*Sievers and Nowlin, 1984; Prézelin et al., 2000*]. Biological hotspots on the WAP are often associated with coastal canyons [*Schofield et al., 2013*]. Canyons are known to enhance upwelling on other continental shelves [*Allen et al., 2001*], and it has been hypothesized that upwelling of UCDW in the WAP canyons is responsible for supporting the thriving biological communities observed there. Upwelling at nearshore canyons can disturb water column stratification, redistributing heat in the surface layer and influencing the concentrations of nutrients, phytoplankton, and sea ice.

The delivery of heat and nutrients to the WAP shelf, and particularly to nearshore areas can profoundly impact biological productivity and rates of glacial and sea ice melt. The aim of this dissertation is to improve our understanding of

some of the delivery processes. The results presented in this dissertation come from a combination of ship-based hydrographic surveys, gliders and mooring observations, and output from a regional numerical model of the WAP. The overall aim of this study is to investigate the delivery mechanisms and pathways of UCDW across the WAP continental shelf.

Chapter 2, which is published in the *Journal of Geophysical Research: Oceans*, investigates the role that subsurface eddies play in delivering heat to the WAP shelf. The importance of this mechanism to the total heat budget of the shelf is evaluated. A spatial overview of eddy locations on the WAP shelf is compiled from four glider deployments completed during three austral summers. Marguerite Trough is confirmed as an important conduit for heat transport and a trough just north of Anvers Island is identified as another pathway of uncertain importance.

In Chapter 3, a regional model of the WAP shelf, developed by Michael Dinniman and John Klinck at Old Dominion University [Dinniman and Klinck, 2004; Graham et al., 2016] is employed to explore the pathways that UCDW follows across the shelf on its way to a nearshore canyon that hosts a productive ecosystem. Palmer Deep, a canyon system that has been extensively studied due to its proximity to Palmer Station and its association with large penguin colonies, is used as a study site. Virtual drifters were initialized along the shelf break and allowed to follow the current velocity field in the model for up to six years. Drifters that ultimately reached the canyon generally moved northward along the continental slope until they were pulled into the shelf interior at one of several cross-shelf troughs. Before entering Palmer Deep, most drifters were caught in the cyclonic circulation of the

trenches offshore and to the north of Anvers Island. The farther north they traveled before looping back into the canyon, the cooler they were when they entered.

In Chapter 4, the nearshore component of UCDW transport to the coast is explored using observations from a subsurface mooring deployed at the head of Palmer Deep. Time series of water column current velocities and bottom temperature are analyzed to understand the role that tides, winds, and circulation patterns have on the flux of heat to this important region. In Chapter 3, the cyclonic circulation of the northern trough systems ended with a southward transport along the west coast of Anvers Island before entering Palmer Deep. This southward flow is also shown to be important in the mooring data, particularly in winter. This observation is in agreement with the proposed leg of the Antarctic Peninsula Coastal Current off Anvers Island that is stronger during winter than summer. Wind forcing was found to have more of an impact on currents at the mooring site during summer.

The final chapter summarizes the results of the dissertation and suggests directions of future research.

2 Distribution of Upper Circumpolar Deep Water on the continental shelf of the West Antarctic Peninsula

2.1 Abstract

We use autonomous underwater vehicles to characterize the spatial distribution of Upper Circumpolar Deep Water (UCDW) on the continental shelf of the West Antarctic Peninsula (WAP) and present the first near-synoptic measurements of mesoscale features (eddies) containing UCDW on the WAP. Thirty-three subsurface eddies with widths on the order of 10 km were detected during four glider deployments. Each eddy contributed an average of 5.8×10^{16} J to the sub-pycnocline waters, where a cross-shelf heat flux of 1.37×10^{19} J yr⁻¹ is required to balance the diffusive loss of heat to overlying winter water and to the near-coastal waters. Approximately two-thirds of the heat coming onto the shelf diffuses across the pycnocline and one-third diffuses to the coastal waters; long-term warming of the sub-pycnocline waters is a small residual of this balance. Sixty percent of the profiles that contained UCDW were part of a coherent eddy. Between 20 and 53% of the lateral onshore heat flux to the WAP can be attributed to eddies entering Marguerite Trough, a feature in the southern part of the shelf that is known to be an important conduit for UCDW. A northern trough is identified as additional important location for eddy intrusion.

2.2 Introduction

Most of the glaciers along the West Antarctic Peninsula (WAP) have retreated since the early 1950s [Cook *et al.*, 2005], and the rate at which ice sheets have been losing mass has accelerated over the past decade [Rignot *et al.*, 2014]. The glacial retreat has been attributed to calving events, linked to warming atmospheric temperatures, and melting from below, attributed to the onshore transport of warmer ocean water [Rignot and Jacobs, 2002; Jenkins *et al.*, 2010; Pritchard *et al.*, 2012; Cook *et al.*, 2016]. Atmospheric temperatures over the WAP have warmed at an approximate rate of 0.5°C per decade since the 1950s [Meredith and King, 2005; Turner *et al.*, 2006; Bromwich *et al.*, 2013], although recent observations show a reversal of the warming trend since the late 1990s, consistent with the large variability of the system [Turner *et al.*, 2016]. Summertime upper ocean water temperatures rose by more than 1°C between the mid-1950s and mid-1990s [Meredith and King, 2005] and continued to increase at a rate of 0.1° - 0.3°C per decade since the 1990s [Schmidtke *et al.*, 2014]. This warming reflects the effects of changes in atmospheric temperatures. Recent observations, however, suggest that glacier retreat on the WAP is driven primarily by deep ocean temperatures [Cook *et al.*, 2016] which can also supply heat to the atmosphere [Venables *et al.*, 2016].

Upper Circumpolar Deep Water (UCDW) is the largest source of ocean heat to the WAP continental shelf [Hofmann *et al.*, 1996]. This water mass is characterized by potential temperatures exceeding 1.7°C and salinities greater than 34.54 [Martinson *et al.*, 2008], and is the warmest deep water mass observed on the WAP continental shelf. UCDW is found just off the shelf at depths between 200 m and 600

m within the Antarctic Circumpolar Current (ACC), an eastward-flowing current that runs directly along the continental slope of the WAP [Klinck, 1998; Klinck *et al.*, 2004]. While surface water properties on the continental shelf vary seasonally with the growth and melting of sea ice and variable wind mixing [Hofmann *et al.*, 1996], water below the permanent pycnocline is kept warm throughout the year by frequent intrusions of UCDW from the offshore ACC [Smith *et al.*, 1999; Martinson *et al.*, 2008].

Overlying the relatively warm deep water on the shelf is Winter Water. This cold water mass is generated from a combination of sea ice growth, sensible heat loss to the atmosphere, and deep vertical mixing driven by winds during the winter and is persistent in most parts of the shelf throughout the summer. In the winter, it extends from the surface to around 200 m. Beginning in the spring, relatively fresh sea ice melt water creates a shallow surface layer that overlies the Winter Water and warms throughout the summer. As UCDW intrudes onto the shelf, it loses heat to the surrounding water and overlying Winter Water through both diapycnal and isopycnal mixing [Smith *et al.*, 1999]. Over the course of the year on the continental shelf, there is a net flux of heat out of the surface ocean with a magnitude estimated between 6 W m^{-2} (using data from 1993 only) [Smith and Klinck, 2002] and 19 W m^{-2} (averaged over 1993-2004) [Martinson *et al.*, 2008]. The cross-pycnocline heat flux from UCDW-warmed water into the Winter Water balances this heat loss to the atmosphere. The temperature gradient that drives this vertical diffusion of heat is preserved by sub-pycnocline along-isopycnal heat transport from off the shelf [Klinck *et al.*, 2004].

Several mechanisms have been suggested for delivering UCDW to the WAP. Upwelling of offshore UCDW is evidenced in hydrographic data by shoaling of the permanent pycnocline [Martinson *et al.*, 2008]. Topographically-induced or wind-driven upwelling events have been linked to large diatom blooms on the shelf [Prézelin *et al.*, 2000]. However, shoaling may not always indicate upwelling; it can also be produced when a subsurface eddy moves onto the shelf and deflects isopycnals [Martinson and McKee, 2012]. Indeed, with the high temporal resolution of mooring observations in Marguerite Trough and the neighboring shelf, and the increased spatial resolution of regional models, mesoscale eddies have emerged as the most prominent mechanism of heat delivery to the WAP shelf [Dinniman *et al.*, 2011; Martinson and McKee, 2012]. While upwelling has not been ruled out as a potential delivery mechanism [Martinson and McKee, 2012], the apparent shelf-wide flooding of UCDW documented in coarsely-resolved hydrographic surveys [Prézelin *et al.*, 2004] was shown to actually be the result of coherent eddies moving on to the shelf and dissipating heat [Moffat *et al.*, 2009; Dinniman *et al.*, 2011; Martinson and McKee, 2012].

Eddies are carried onto the shelf during episodic advective intrusions of UCDW, which may occur during periods of intense wind stress [Dinniman *et al.*, 2011]. Modeling studies and observations indicate that, with a strong enough forcing, when the mean shelf break flow encounters curving bathymetry, some of the water flowing in the ACC along the shelf break is carried by momentum onto the shelf [Dinniman and Klinck, 2004; Klinck *et al.*, 2004]. Evidence from a high-

resolution model also suggests that Rossby waves at the shelf break can interact with a trough to produce features consistent with eddies [*St-Laurent et al.*, 2013].

Moorings in Marguerite Trough and on the surrounding shelf have recorded eddies passing by at rates of three to four per month [*Moffat et al.*, 2009; *Martinson and McKee*, 2012], but presence elsewhere on the shelf is largely unknown. Existing datasets in the region were collected using traditional shipboard sampling, with measurements typically made at coarser resolution than that required to resolve mesoscale eddies on the WAP. Weak subsurface stratification of the shelf combined with the effects of high latitude result in a small radius of deformation which determines the length scale of eddy dynamics [*Chelton et al.*, 1998]. Eddies shed from the ACC have diameters of $\sim 10\text{-}20$ km [*Klinck and Dinniman*, 2010].

Here, we use data from four deployments of Slocum-Webb autonomous underwater vehicles (gliders) to map the spatial distribution of UCDW on the shelf. Some of the UCDW is contained in subsurface mesoscale eddies with widths on the order of 10 km. Glider profiles are 1 km apart, on average, providing sufficient spatial resolution to define the horizontal boundaries of mesoscale features. These data allow us to identify previously undetected pathways of intrusion for eddies onto the shelf, and allow us to estimate their relative importance to the WAP continental shelf heat budget.

We place these glider deployments in the context of annual shelf-wide hydrographic data from repeat cruises conducted each January from 1993 to 2008 [*Smith et al.*, 1995b; *Ducklow et al.*, 2012]. Hydrographic stations occupied during these cruises were rarely closer than 20 km apart, so they lack the spatial resolution

to detect eddies on the shelf, but they allow us to construct a sub-pycnocline heat budget from which we can estimate the contribution of subsurface eddies carrying UCDW and discuss their impact on the warming trend observed across the shelf over the last several decades.

2.3 Methods

This study uses data obtained from four deployments of Slocum Webb deep gliders from Palmer Station, Antarctica ($64^{\circ}46'S$, $64^{\circ}03'W$) during austral summers 2010-11, 2011-12, and 2012-13. Deployments lasted between 29 and 62 days and covered distances up to 1600 km in the coastal waters west of the Antarctica Peninsula (Figure 2-1). Gliders are buoyancy-driven autonomous underwater vehicles that move from the surface to a depth of up to 1000 m with an average horizontal speed of 1 km hr^{-1} [Davis *et al.*, 2002; Schofield *et al.*, 2007]. All gliders used in this study were equipped with a Seabird CTD to measure conductivity, temperature, and depth with a sampling resolution of 4-6 measurements per vertical meter. Data from each dive or climb were averaged into 1 m depth bins and the latitude/longitude of the entire profile was set to the average latitude/longitude of the climb or dive.

In each of the four deployments, gliders traveled generally southward along the peninsula. We restrict our focus to profiles taken on the continental shelf, which we define as shoreward of the 600 m isobath (Figure 2-1 a). Among the shelf profiles, UCDW ($T > 1.7^{\circ}\text{C}$ and $S > 34.54$, [Martinson *et al.*, 2008]) was often encountered below the permanent pycnocline as part of distinct boluses with

characteristics consistent with subsurface eddies (Figure 2-1 b).

Studies of subsurface eddies in the North Pacific [Pelland *et al.*, 2013] and North Atlantic [Bower *et al.*, 2013] suggest that a Gaussian distribution model is appropriate for defining the horizontal boundaries of those features. We use it to measure chord lengths of the eddy-like boluses encountered by the gliders. From

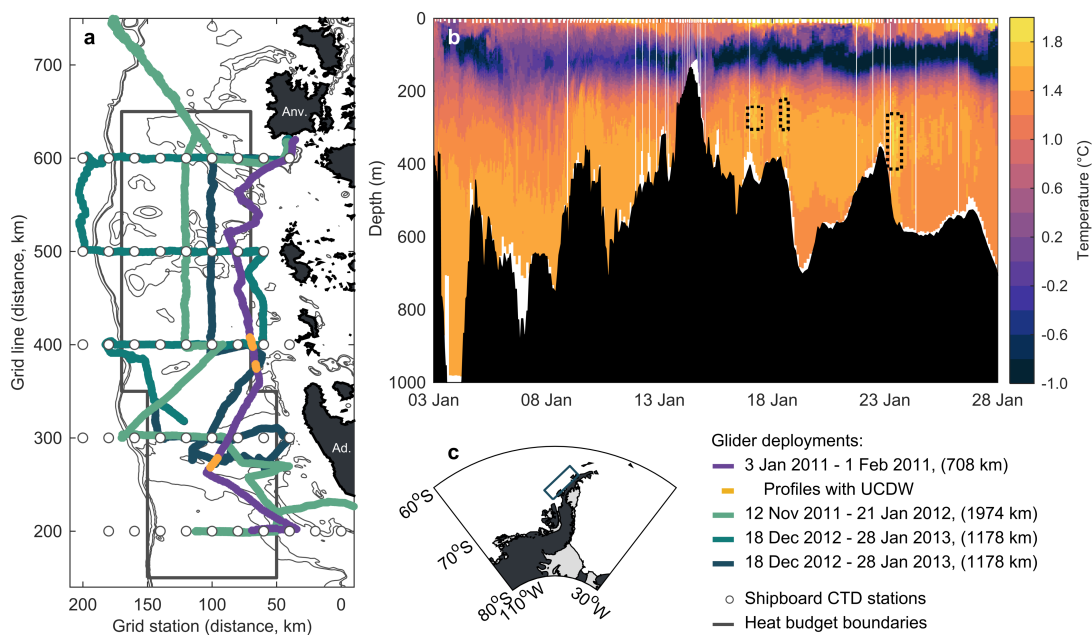


Figure 2-1: Map WAP continental shelf and glider tracks.

(a) The region of the WAP continental shelf discussed in this analysis. Shipboard CTD profile locations used in the heat budget calculations are shown as circles. The gray box encloses stations used to calculate the change in shelf heat over time and the vertical heat flux to the winter water layer. Lateral diffusion is measured across the right box boundary and lateral onshore heat flux is calculated across the left box boundary. Green and purple lines show tracks of the four glider deployments. Temperature data from the purple track are shown in panel b with yellow dots indicating profiles where UCDW was found. Bathymetry contours are plotted at the 500, 600, and 1000 m isobaths. Anvers (Anv.) and Adelaide (Ad.) Islands are labeled. (b) Temperature section from the glider deployment shown in purple in panel a. Dotted boxes show the extent of UCDW in the three mesoscale features detected on this deployment. (c) Regional map, with boundaries of panel a shown.

here forward, we will refer to the boluses as “eddies.” The model assumes that the cross-section of an eddy along an isopycnal is circular and that its temperature is greatest at its center and decays in the radial direction. This geometry is described by the following equation:

$$T' = T_{\max} \cdot e^{-\left(\frac{(x-x_0)}{r}\right)^2}, \quad (2-1)$$

where T' is the temperature anomaly at position x , T_{\max} is the maximum value of the anomaly at the eddy center, x_0 , and r is the eddy radius.

Following the methods of Zhang et al. [2015], who calculated widths of sub-thermocline eddies in the North Pacific using Argo float profiles, we interpolated temperature profiles onto surfaces of constant potential density separated by 0.01 kg m^{-3} . For each isopycnal surface, using only observations on the shelf, we calculated the mean temperature and anomalies from the mean. We then identified every shelf profile that contained UCDW at any depth and fit Gaussian curves to the positive temperature anomalies surrounding these profiles on each of fifteen isopycnal surfaces between $1027.63 \text{ kg m}^{-3}$ (approximating the base of the winter mixed layer and the shallowest isopycnal where UCDW was found) and $1027.77 \text{ kg m}^{-3}$ (the deepest isopycnal that at least 50% of glider profiles extended to).

We used the MATLAB ‘fit’ function to calculate the radii of the eddies according to Equation 2-1 (Figure 2-2). Distances (x) were measured along the least-squares fit line through all points on the isopycnal surrounding the UCDW profile that had positive temperature anomalies (Figure 2-2 a). This method was repeated for every profile containing UCDW and every potential density surface

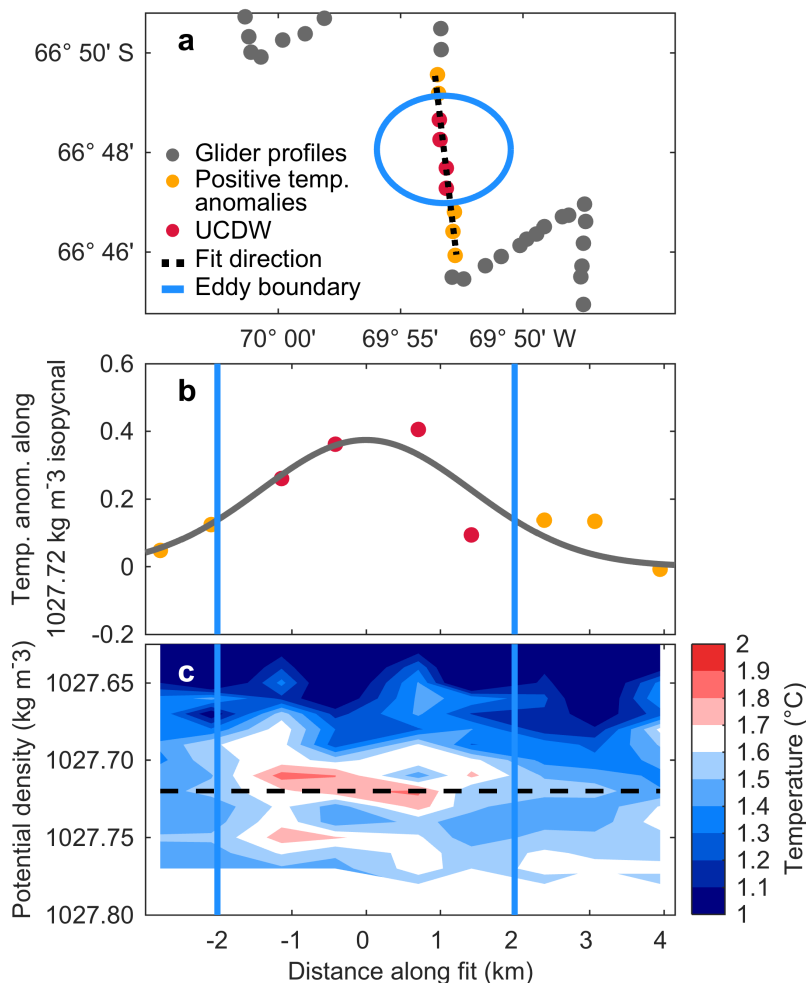


Figure 2-2: Example of method used to define eddy width.

(a) Profiles containing UCDW at any depth are identified based on temperature and salinity values (red dots). One isopycnal surface is selected and the surrounding profiles that contain positive temperature anomalies along that surface are identified (yellow dots). A least-squares line is fit to these profiles (black dashed line). (b) A Gaussian curve is fit to the positive temperature anomalies along the chosen isopycnal in the direction of the least squares fit. Eddy width is defined by Equation 2-1 as twice the radius, enclosing 84.3% of the heat (vertical blue lines). (c) Temperature section with vertical blue lines showing the calculated eddy width. Dots in panels a and b show the locations of each glider profile (a single dive or climb).

between 1027.63 and 1027.77 kg m⁻³, resulting in several fits to the same feature;

we chose the best as the fit with the lowest rms/mean.

Isopycnals representing the best fits ranged from 1027.70 to 1027.76 kg m⁻³.

Eddy chord lengths were defined according to Equation 2-1 as twice the radius, r , which encloses 84.3% of the temperature anomaly in the fit (Figure 2-2b). These lengths are used as an estimate for eddy width, but since we do not know how closely the glider passed through eddy centers, nor do we know the direction of eddy movement, there is error in this estimate. Drawing random lines through a stationary circle to measure the diameter would result in an average estimate that is 68% of the true diameter, but eddies are not assumed to be stationary during the time the glider spent sampling them. Width is likely to have been underestimated (overestimated) during times when the glider passed through an eddy as it was carried by the mean flow in the opposite (same) direction as the glider motion.

The heat content of each eddy was calculated relative to the average shelf temperature, T_{ref} :

$$Q = \int (T - T_{ref}) \rho_z c_p \pi r^2 dz, \quad (2-2)$$

where z_1 and z_2 are the shallowest and deepest depths where UCDW was observed within a single eddy. These depths averaged 221 m and 346 m on the shelf across all glider deployments. The reference temperature, T_{ref} , was calculated as the average potential temperature below the permanent pycnocline of all non-UCDW profiles on the shelf and had a value of 1.2 °C. Since the reference temperature includes every profile where the maximum potential temperature was below 1.7 °C and doesn't demand that the profile be cooled any further, heat calculated relative to this temperature represents a lower bound of the heat delivered to the shelf by eddies.

Temperature profiles were also taken during annual cruises in January 1993 and 1995-2015 as part of the Palmer Long Term Ecological Research (LTER) project. The LTER grid is made up of lines running along the peninsula spaced 100 km apart and stations running perpendicular to the shelf spaced 20 km apart (Figure 2-1 a). The lines are named according to distance from a point south of this particular study area: the 200 line extends out from south of Adelaide Island and, 400 km northeast of that, the 600 line extends out from south of Anvers Island (Figure 2-1). The same temperature and salinity criteria ($T \geq 1.7^{\circ}\text{C}$, $S \geq 34.54$) used to identify UCDW in the glider data were used to identify UCDW in the shipboard CTD data, and the same potential density surfaces were used to calculate the heat content of every profile. These data were used to investigate the spatial patterns of UCDW on the shelf. They were also used to create a volume-averaged heat budget for the WAP shelf in order to determine the importance of the subsurface eddies as a source of heat to the shelf.

2.4 Results and Discussion

2.4.1 Locations of UCDW intrusions

Hydrographic measurements on the WAP, taken from both traditional ship platforms and glider deployments, reveal a consistent pattern of intrusion locations onto the shelf (Figure 2-3). Both data sets show a heightened presence of UCDW on the shelf in deep areas, mostly confined to the region around Marguerite Trough (300 and 400 lines). In both data sets, observations of UCDW drop off with distance from the shelf break toward the coast, as expected, since processes on the shelf lead

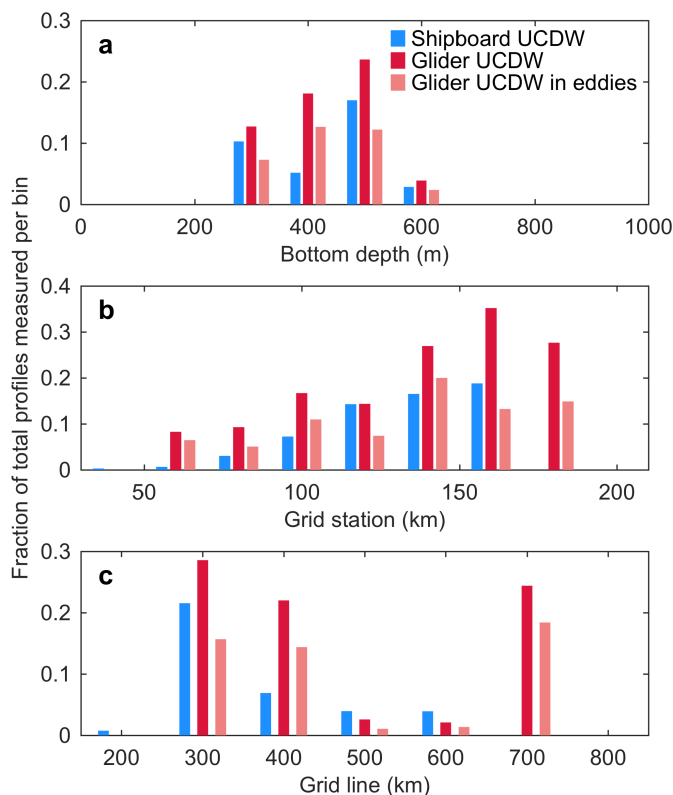


Figure 2-3: Histograms of UCDW detected on the shelf. Fractions of (blue) total shipboard CTD profiles that contained UCDW, (red) total glider CTD profiles that contained UCDW, and (pink) total glider CTD profiles that were part of an eddy, that were found in bins of (a) bottom depth, (b) grid station, and (c) grid line. Eddy profiles were identified by fitting Gaussian curves to temperature anomalies, as described in section 2.

to the modification of UCDW.

Ocean gliders have significantly improved the spatial resolution of hydrographic measurements along the Antarctic Peninsula, allowing us to resolve features smaller than the spacing of a typical ship-based survey [Heywood *et al.*, 2014; Erickson *et al.*, 2016]. The increased sampling resolution of the gliders increases the likelihood of encountering the small-scale features containing UCDW. The glider data confirm our understanding of UCDW intrusion locations but indicate that studies based solely on hydrographic surveys with profiles separated by 20 km

or more have underestimated the quantity of unmixed UCDW on the shelf (Figure 2-3, blue bars vs. red bars). During some LTER cruises, no UCDW was seen on the shelf, but it easily could have been missed; a single CTD cast from a ship is meant to represent a 20 km x 100 km area of ocean, within which it is possible for several mesoscale features to exist but go undetected. Glider surveys consistently encountered more UCDW per unit effort (profiles measured) than did shipboard surveys.

The glider data allow us to separate UCDW that appears in coherent eddies from UCDW present outside eddy-like structures. Coherent features carrying UCDW were seen in each of the four glider deployments. Of all profiles containing UCDW, 60% occurred as part of eddies (Figure 2-3, pink bars vs. red bars). The UCDW found outside of eddies was present either near the shelf break spread over tens of kilometers, which may be evidence of a mean advection across the shelf break, or as isolated profiles near the locations where eddies were found, which may represent remnants of larger features that had dissipated or instances of interleaving.

Mooring observations from the vicinity of Marguerite Trough previously identified eddies there [*Moffat et al., 2009; Martinson and McKee, 2012*]. Glider observations confirm that this canyon is important for the advection of eddies onto the shelf and identify an additional, previously undetected, intrusion pathway to the north. The “northern canyon” (Figure 2-4a). is a cross-shelf canyon that lies outside the boundaries of the LTER grid, so no observations of UCDW had been made there during the LTER time-series of shipboard CTD profiles. Mesoscale features containing UCDW were, however, observed along the northern wall of this canyon in

the glider data. Similarly, UCDW eddies were found along the northern wall of the entrance to Marguerite Trough. Eddies that enter the shelf at Marguerite Trough appear to follow one of two pathways onto the shelf: an upper pathway follows the 400 m isobaths to the northeast and a lower pathway follows the 500 m isobaths the southeast (Figure 2-4 a). The highest percentage of UCDW on the shelf was measured in areas with depths near 500 m (Figure 2-3 a), which is the approximate depth of both Marguerite Trough and the northern canyon where they cross the shelf break.

2.4.2 Properties of UCDW eddies

Overall, 14% of the profiles measured by the gliders on the shelf contained UCDW. Of these, 60% were contained in 33 coherent Gaussian features with properties consistent with subsurface eddies. The majority of these features were found in or around Marguerite Trough, but the northern canyon also appears to be a conduit for transport of eddies onto the shelf (Figure 2-3 a). Fewer observations were made in that canyon than in Marguerite Trough.

The mean value of all chord lengths was 11.3 ± 5.1 km with a median value of 10.3 km. It is important to note that eddy widths measured here are an estimate of true diameters since we do not know how close the glider came to the center or the direction of eddy travel. However, these estimates are within the range of eddy sizes predicted by the internal deformation radius [*Chelton et al.*, 1998] and are similar to the size of eddies measured by moorings on the shelf [*Moffat et al.*, 2009; *Martinson and McKee*, 2012].

Subsurface eddies entering the shelf contained as much as 1.93×10^{17} J of heat relative to the reference temperature (1.2 °C). Eddies lose heat to the overlying winter water and to the cooler shelf waters as they are carried in the mean flow. In the general circulation pattern in the southern half of the grid, water enters onto the shelf through Marguerite Trough and makes a counter-clockwise loop following the northern branch of the canyon [Smith *et al.*, 1999; Dinniman and Klinck, 2004; Savidge and Amft, 2009]. A second branch carries water into Marguerite Bay via the southern branch of the canyon [Klinck *et al.*, 2004]. The properties of eddies detected by the gliders are consistent with this pattern.

In Figure 2-4, panels b-e show properties of eddies that enter Marguerite Trough as a function of distance from the shelf break along one of two isobaths. Heat content per unit area and height are most strongly correlated with distance. Eddy height is defined as the vertical distance separating the shallowest and deepest observations of UCDW within the eddy. Radius and average temperature are weakly correlated with distance. Again, the interpretation of these relationships must include a consideration of the chord-length sampling error. An eddy that a glider passed through the edge of would appear to have a shorter radius and a cooler average temperature than if the eddy had been sampled through the middle. The observations suggest that subsurface eddies enter onto the shelf with widths on the order of 10 km and are modified as they travel along an isobaths. They dissipate heat both vertically and laterally. Slower rates of lateral diffusion and the resulting effects of lateral spreading may explain the weak correlation between eddy width and distance traveled.

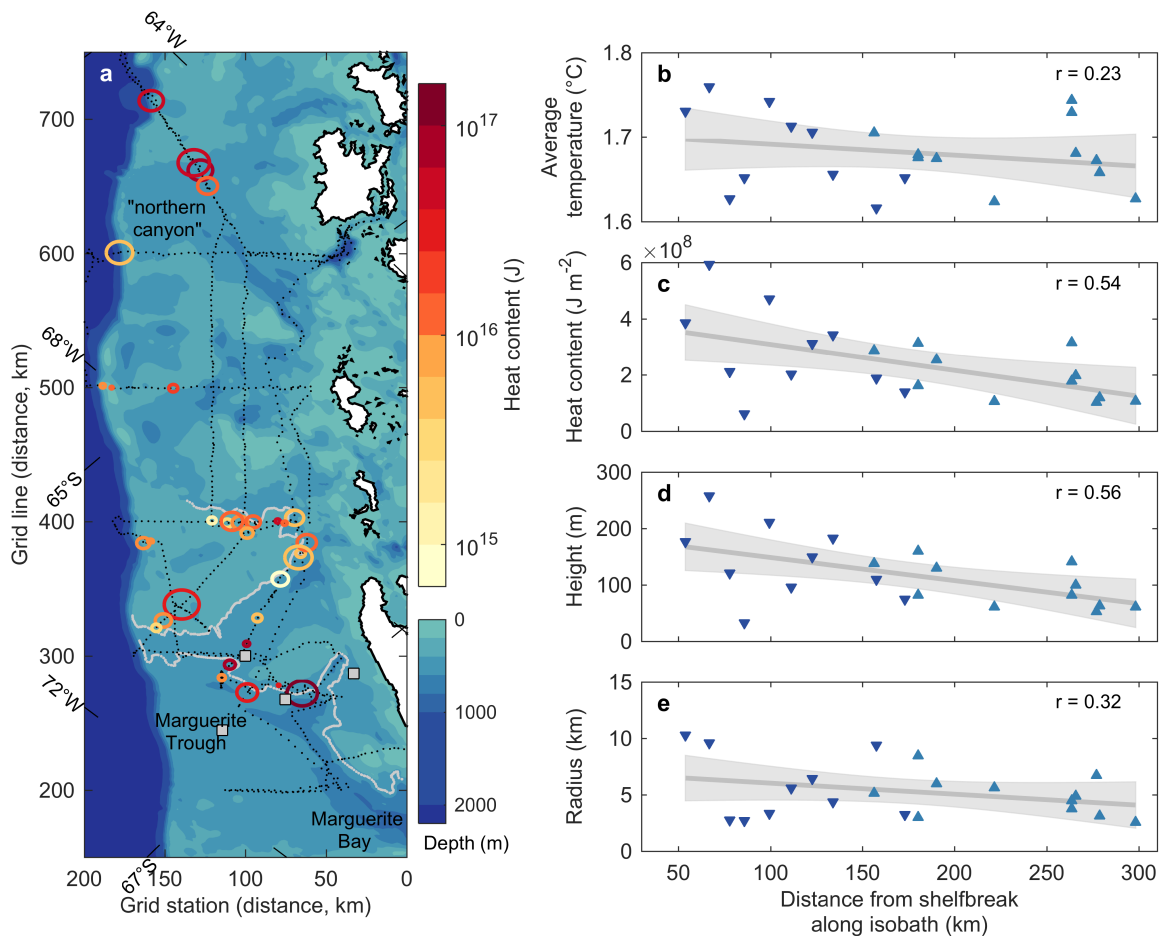


Figure 2-4: Map and characteristics of eddies on the WAP shelf.

(a) Map of WAP continental shelf with overlaid eddies detected by the gliders, colored by the average heat content of the profiles measured within them. Dotted black lines show glider tracks. Grey squares show the locations of SO GLOBEC moorings [Moffat *et al.*, 2009] and LTER [Martinson and McKee, 2012] moorings that have been used in previous studies to measure frequency of eddy intrusion into Marguerite Bay. Gray lines trace the 400 m (upper) and 500 m (lower) bathymetric contours representing “upper” and “lower” paths of Marguerite Trough. Dark blue downward-pointing triangles in panels b-e show data from eddies lying along lower contour, and light blue upward-pointing triangles show data from eddies lying along upper contour. Gray lines and shading in panels b-e represent least-squares fit to data and 95% confidence bounds. Correlation coefficients are given.

2.4.3 Heat balance on the WAP

A simple two-dimensional heat budget was constructed for the region of the WAP shelf where glider and CTD observations were made (Figure 2-5). This region extends 500 km along the coast and 100 km across the continental shelf (Figure 2-1 a). Vertical limits are between the depth of the permanent pycnocline, which has an average depth of 160 m and generally corresponds to the $1027.63 \text{ kg m}^{-3}$ isopycnal, and the seafloor, which are separated by an average distance of 280 m. The height of the heat budget box is defined as this average distance. Following the assumption of Klinck et al. [2004], we assume the alongshore advection is small and that there is no heat flux at the bottom or directly at the coast, although we do calculate lateral diffusion between the mid-shelf and nearshore stations. The heat balance below the permanent pycnocline on the shelf is the sum of lateral fluxes across the shelf break, diapycnal diffusion into the overlying winter water, and isopycnal diffusion across the shoreward box boundary (Figure 2-1 a). Here, we extend the analysis to include all years between 1993 and 2008, during which the overall heat content of the shelf increased [Martinson et al., 2008]. Therefore, we also include a shelf warming term. Temperatures below the permanent pycnocline on the WAP shelf during the 1993-2008 sampling period warmed at an average rate of $0.01 \text{ }^\circ\text{C}$ per year.

We integrate the advection-diffusion equation over the width (L) and depth (H) of the shelf, ignoring vertical advection and including a warming trend. We then divide by the width and depth to arrive at the volume-averaged heat budget equation:

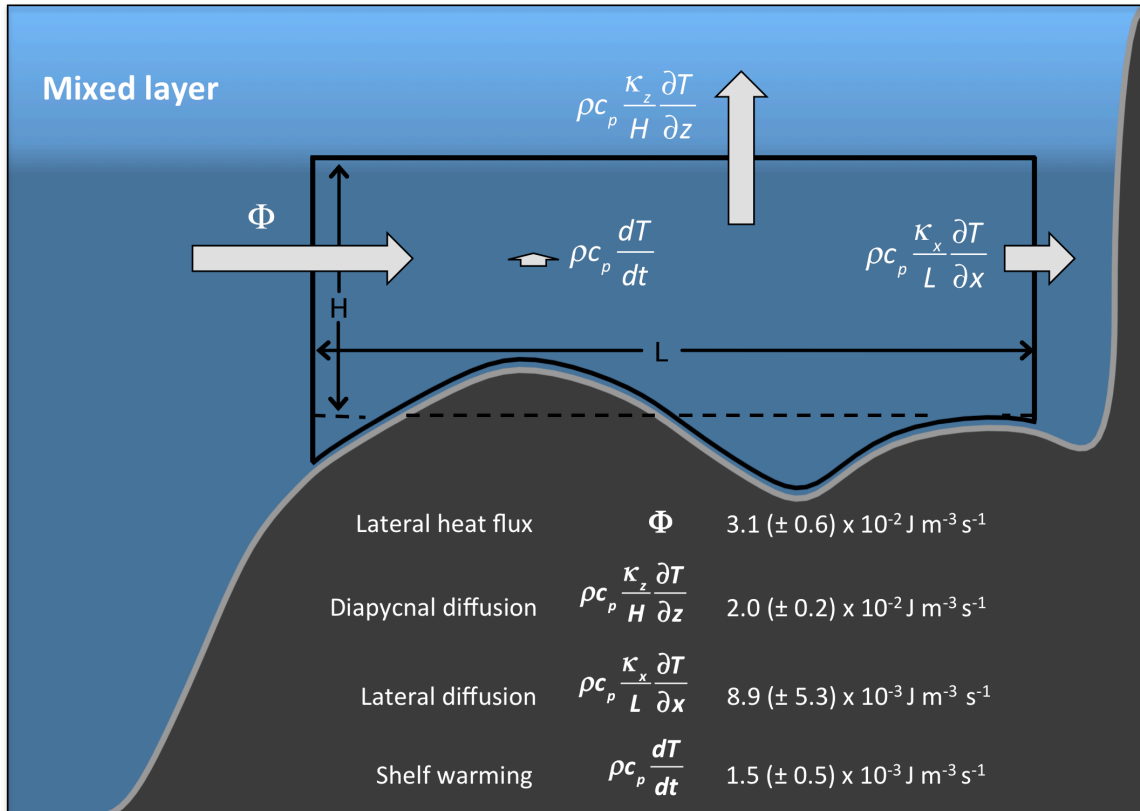


Figure 2-5: Schematic illustrating the components of the heat budget on the WAP continental shelf.

Values shown are calculated using $\kappa_x = 100 \text{ m}^2 \text{ s}^{-1}$. All other values are listed in Table 2-1. We use the average bottom depth of the WAP, indicated by the dashed line, as height, H . Arrow lengths are proportional to the relative contributions of each term to the heat budget.

$$\Phi - \rho c_p \left(\frac{\kappa_z}{H} \frac{\partial T}{\partial z} + \frac{\kappa_x}{L} \frac{\partial T}{\partial x} \right) = \rho c_p \frac{dT}{dt} \quad (2-3)$$

The lateral temperature gradient, $\frac{\partial T}{\partial x}$, is the time-series average gradient of

temperatures between mid- and inner-shelf stations. Similarly, $\frac{\partial T}{\partial z}$ is the shelf-wide

time-average temperature gradient across the permanent pycnocline at each

station. H is the average vertical distance between the permanent pycnocline and the seafloor and Φ is the total flux across the shelf break. Values for all heat budget terms are listed in Table 2-1: Coefficients and variables used for heat budget calculations.

Table 2-1: Coefficients and variables used for heat budget calculations.

| Symbol | Description | Value |
|---------------------------------|---|--|
| T_{ref} | reference seawater temperature | 1.2 °C |
| ρ | reference seawater density | 1027.7 kg m ⁻³ |
| c_p | specific heat of seawater | 4000 J kg ⁻¹ °C ⁻¹ |
| H | height of heat budget box | 280 m |
| L | across-shelf extent of heat budget box | 100 km |
| W | along-shelf extent of heat budget box | 500 km |
| κ_z | vertical diffusivity | 10 ⁻⁴ m ² s ⁻¹ |
| κ_x | lateral diffusivity | 100 (37, 200) m ² s ⁻¹ |
| $\frac{\partial T}{\partial t}$ | time rate of change of shelf temperature | 3.61 (± 1.15) x 10 ⁻¹⁰ °C s ⁻¹ |
| $\frac{\partial T}{\partial x}$ | mid- to inner- shelf temperature gradient | 2.18 (± 1.28) x 10 ⁻⁶ °C m ⁻¹ |
| $\frac{\partial T}{\partial z}$ | diapycnal temperature gradient | 0.014 ± 0.002 °C m ⁻¹ |

Values for the lateral and vertical diffusivities, κ_x and κ_z respectively, are taken from the literature. Howard et al. [2004] estimated a shelf-wide average diapycnal diffusivity of 10⁻⁵ m² s⁻¹ based on fall and winter cruises in 2001, however this value is thought to underestimate the true mixing on the shelf which is dominated by isolated wind events [Howard et al., 2004]. Estimates based on shelf-wide budgets suggest a value closer to 10⁻⁴ m² s⁻¹ [Klinck, 1998; Smith et al., 1999; Smith and Klinck, 2002; Martinson et al., 2008] and not exceeding 7.7 x 10⁻⁴ m² s⁻¹

[*Klinck et al., 2004*]. As the shelf waters have warmed, the magnitude of κ_z has decreased [*Martinson et al., 2008*]. We use $10^{-4} \text{ m}^2 \text{ s}^{-1}$ as an average value for the shelf over the time series, which leads to an appropriate eddy-decay time scale of eddies advected with the mean flow in Marguerite Trough [*Moffat et al., 2009*]. Estimates of isopycnal diffusivity on the shelf range from $37 \text{ m}^2 \text{ s}^{-1}$ [*Klinck, 1998*] to $200 \text{ m}^2 \text{ s}^{-1}$ [*Smith et al., 1999*] to an unrealistic maximum of $1600 \text{ m}^2 \text{ s}^{-1}$ [*Klinck et al., 2004*]. According to mixing length arguments, lateral diffusivity scales as $\kappa \sim vl$ [*Prandtl, 1925*]. Using a typical sub-pycnocline current speed of $1\text{-}5 \text{ cm s}^{-1}$ [*Howard et al., 2004; Klinck et al., 2004*] and a typical eddy width of 10 km, mixing length arguments indicate that lateral diffusivity should be on the order of $100\text{-}500 \text{ m}^2 \text{ s}^{-1}$. This gives us confidence to use the $37\text{-}200 \text{ m}^2 \text{ s}^{-1}$ range in our calculations.

Using values listed in Table 2-1: Coefficients and variables used for heat budget calculations, we calculate the average diapycnal diffusion across the permanent pycnocline, the average lateral diffusion across the inner heat box boundary, and the rate of shelf warming over the 1993-2008 shipboard sampling period. The magnitude of diapycnal diffusion is about twice that of lateral diffusion and the shelf warming term is, comparatively, very small. Of the heat that enters the shelf below the permanent pycnocline, approximately two-thirds is diffused vertically across the permanent pycnocline and one-third reaches the coastal waters by lateral diffusion.

We calculate the horizontal lateral flux, Φ , required to balance the other terms, to be $1.36 \times 10^{19} \text{ J yr}^{-1}$ (ranging from $0.97 \times 10^{19} \text{ J yr}^{-1}$ to $2.23 \times 10^{19} \text{ J yr}^{-1}$ depending on the lateral diffusivity, and including error estimates). This value is

found by multiplying Φ in Eq. 3 by the volume of the heat budget box, and represents the total lateral heat flux from various mechanisms, including eddies transported onto the shelf. The average heat content of eddies observed near the shelf break is 5.8×10^{16} J. The total annual heat flux onto the shelf is equivalent to 150-342 eddies with an average temperature of 1.7°C across a diameter of 12 km (the average temperature and width of observed eddies within 50 km of the shelf break) coming onto the shelf each year.

Year-round mooring observations at a fixed location north of Marguerite Trough led to estimates that 35-40 eddies containing UCDW passed by the mooring location each year during 2007, 2008, and 2010 [*Martinson and McKee, 2012*]. Observations from a mooring shoreward of that location, within the trough itself, showed similar numbers of eddies passing there [*Moffat et al., 2009*]. Our results show that eddies occur at similar densities to the north and south of the Marguerite Trough entrance so, assuming the trough is a conduit for 70-80 eddies per year, it alone could serve as the entryway for 20-53% of the necessary heat flux to the shelf. The northern canyon appears to be an additional location of eddy intrusion, although further observations there will be necessary to quantify its contribution as an eddy delivery pathway. In 186 days on the shelf, our gliders encountered 33 eddies suggesting that a lower-limit estimate of eddy intrusions onto the WAP shelf each year is around 64, which would account for 19-43% of the range of lateral heat flux estimates.

2.5 Conclusions

High-resolution measurements from Slocum Webb deep gliders deployed along the west Antarctic Peninsula confirm that warm water from the ACC is intruding onto the continental shelf as distinct mesoscale features [Moffat *et al.*, 2009; Martinson and McKee, 2012; St-Laurent *et al.*, 2013; Graham and Dinniman, 2016]. The high spatial resolution of the glider data allows us to present the first near-synoptic cross-sections of mesoscale eddies on the WAP. We estimate the eddy-like boluses to be on the order of 10 km wide and 125 m thick. Intrusions tend to occur at Marguerite Trough and a second cross-shelf canyon in the northern part of the study area. The annual shipboard CTD measurements also indicate these two canyons act as primary conduits for heat transport, but they are unable to resolve the spatial extent of the intrusions.

Glider measurements have allowed us to capture warm water features over a larger area of the WAP continental shelf than was previously available, but we still lack information about the mechanism by which the warm deep water, once on the shelf, reaches the coastal surface waters. Recent research using gliders suggests that bathymetry plays an important role in local mixing of deep and surface waters and may be important in the transformation of water masses across the entire shelf [Venables *et al.*, 2016]. Melting of the glaciers on the West Antarctic Peninsula could raise global sea levels by up to 69 ± 5 mm [Huss and Farinotti, 2014] and most of the glacier retreat since the 1990s can be attributed to interactions with the ocean [Cook *et al.*, 2016]. Understanding the rate at which heat contained in the ocean is melting the ice is crucial to predicting how much ice will be lost in the warming

climate. The UCDW features described here may account for up to 50% of the onshore heat flux, with the remainder likely to come from upwelling and advection of the ACC onto the shelf. Future efforts will focus on a better understanding of the eddy dissipation processes and the mechanisms responsible for bringing the remaining heat to the shelf.

3 Pathways and retention times in a biologically productive canyon system on the West Antarctic Peninsula

3.1 Abstract

Palmer Deep is a highly productive coastal canyon on the continental shelf of the West Antarctic Peninsula (WAP), located near the United States operated field station, Palmer Station. Primary productivity in the canyon is hypothesized to be fueled by nutrients provided by Upper Circumpolar Deep Water (UCDW), a water mass originating off the shelf. To evaluate the influence of UCDW on the canyon, we use an the Regional Ocean Modeling System (ROMS) simulation to investigate the UCDW pathways to Palmer Deep and the circulation of the water mass within the canyon itself. Virtual drifters were advected in the velocity field of a six-year model run on the WAP. At sub-pycnocline depths, three primary pathways from the northern shelf edge to Palmer Deep were identified, each including cyclonic circulation within a shelf-incising trough. Temperature and salinity of water moving along these pathways was most significantly modified when it reached the latitude of Boyd Strait, which is likely to be influenced by cold Antarctic Coastal Current Water from the Weddell Sea. Locally within Palmer Deep, most of the flow into the canyon occurred on the northwest side and most of the outflow was to the south. Retention times in the canyon increased with depth, with surface particles retained for up to 15 days and particles at depths where modified UCDW (mUCDW) commonly intrudes retained for 50-100 days. These long retention times of mUCDW

support the idea that canyons promote productivity by providing a reservoir for nutrient-rich water masses.

3.2 Introduction

On the continental shelf of the west Antarctic Peninsula (WAP), regions of high primary productivity, or “biological hotspots,” are thought to be supported by the upwelling of a relatively warm and nutrient-rich water mass that originates off the shelf. Upper Circumpolar Deep Water (UCDW) is found between depths of 200 m and 600 m at the poleward edge of the Antarctic Circumpolar Current (ACC) which travels northward along the WAP shelf break [*Hickey, 1995; Klinck, 1998; Klinck et al., 2004*]. Carrying excess heat and nutrients [*Prézelin et al., 2000*], UCDW enters onto the shelf through cross-cutting troughs that open at the shelf break. Vertical mixing of UCDW with Winter Water and Antarctic Surface Water is variable in time and space and is influenced by bathymetry, winds, tides, sea ice, and stratification [*Klinck, 1998; Smith and Klinck, 2002; Dinniman and Klinck, 2004; Wallace et al., 2008*]. Thus, UCDW is modified by the time it moves across the shelf to coastal canyons, but is still warm and nutrient-rich compared to overlying water masses. Modified UCDW (mUCDW) extends across the entire WAP shelf to very near coastal waters [*Smith et al., 1995a*].

Canyons on the WAP shelf are hypothesized to act as both conduits and reservoirs for modified UCDW. The accumulation of UCDW in canyons promotes primary productivity via a number of mechanisms: 1) warm water upwelled from depth at the head of canyons promotes sea ice melt, which increases stratification, creating a

well-lit mixed layer for phytoplankton [*Kavanaugh et al., 2015*], 2) the stable mixed layer is also replete with nutrients delivered by the upwelled UCDW [*Kavanaugh et al., 2015; Henley et al., 2017*], and 3) circulation within canyons can trap water, leading to long retention times allowing more opportunity for nutrients to be utilized [*Kavanaugh et al., 2015*].

Palmer Deep is a highly productive, deep coastal canyon located approximately 100 km shoreward of the shelf break and just south of Anvers Island (Figure 3-1). Despite its distance from the ACC, Palmer Deep contains a reservoir of mUCDW beneath the winter mixed layer, and productivity over the canyon has been shown to be elevated in regions where warm water is upwelled toward the surface layer [*Schofield et al., 2013*]. Beyond creating an ideal environment for phytoplankton growth, submarine canyons are known to concentrate krill and small fish [*Mackas et al., 1997; Lavoie et al., 2000; Allen et al., 2001*], which support penguins, whales, and seals on the WAP. Westerly winds in the vicinity of Palmer Deep are correlated with increased biomass of krill near shore, suggesting that temporally transient near-shore aggregations are caused by wind-driven transport from the canyon [*Bernard et al., 2017*].

Although Palmer Deep is known to be an important biological hotspot on the WAP, the retention time of this canyon and the associated circulation pathways are considerably less well understood than other hotspots on the shelf. Marguerite Trough, in the southern part of the WAP shelf region (Figure 3-1), is associated with several biological hotspots near the coast. These locations have high particle retention times (18-35 days) [*Piñones et al., 2011*] sufficient to increase

phytoplankton biomass and promote zooplankton population growth [Genin, 2004]. The concentration of chlorophyll-a biomass over Palmer Deep is substantially elevated compared to the shelf areas [Kavanaugh *et al.*, 2015]. The productivity of this canyon may similarly be explained by the long retention time of nutrient-dense water masses.

Pathways delivering UCDW to Palmer Deep are also poorly understood. Observations from hydrographic measurements and Acoustic Doppler Current Profiler (ADCP) surveys [Savidge and Amft, 2009] indicate that flow across the shelf predominantly follows bathymetry. Prézelin *et al.* [2000] showed that diatom-dominated phytoplankton assemblages occurred at several locations where UCDW was upwelled by bathymetry near the shelf break into the surface waters. These locations coincided with areas where the southern boundary of the ACC was nearest the shelf. Small cyclonic features exist at the troughs that open at the shelf break; water flows in along the northern sides and out along the southern sides [Dinniman and Klinck, 2004]. One such trough bisects the shelf, opening at a depth of ~500 m at the shelf break and connecting to the mouth of Palmer Deep (Figure 3-1). Mean currents within this feature, derived from 6 years of ADCP measurements, are generally southward, parallel to the west coast of Anvers Island, in both the 40-200 m and the 200-400 m depth bins. At the deepest part of the canyon mouth, mean currents turn to flow toward the head of the canyon [Savidge and Amft, 2009].

These temporally averaged current fields suggest a probable entrance to Palmer Deep is along the shelf-incising trough that runs from the shelf break toward the mouth of Palmer Deep, which we refer to as the “northern trough.” This region

of the shelf has been identified as one of only two areas along the shelf break where UCDW intrudes onto the shelf [Prézelin *et al.*, 2004], where there is enough curvature of the shelf break to induce advection of UCDW onshore [Dinniman and Klinck, 2004]. Both these locations are associated with shelf-cutting troughs where above-average diatom abundances have been observed, thought to be fueled by the nutrient-rich UCDW funneled along the deep bathymetric features [Prézelin *et al.*, 2004]. However, water intruding down these pathways tends to first enter the shelf upstream [Dinniman and Klinck, 2004] and travel northward at the shelf edge. From here, currents can be deflected shoreward where the bathymetry curves significantly at these two locations. A model study of the WAP showed that intrusions onto the shelf occur more frequently when along-slope current velocities are strong [Dinniman *et al.*, 2011]. A model study of Pine Island Bay showed increased intrusions with stronger westerly winds [Thoma *et al.*, 2008], which could be associated with accelerations in the slope flow.

Current velocity climatologies provide no information about the variability in delivery pathways to Palmer Deep, about the amount of time required for UCDW to travel from the shelf break to the canyon, or about upwelling within the canyon itself. The aim of this study is to estimate the residence time of water in Palmer Deep and the circulation pathways that lead to the canyon, particularly at the depths where modified UCDW is commonly found. To answer these questions, we released virtual Lagrangian drifters in the circulation field of a high-resolution numerical circulation model of the WAP shelf.

3.3 Model Description

A regional ocean model of the WAP was used to investigate the circulation within Palmer Deep and the pathways traveled by UCDW from the shelf break to the canyon. The model used here is a 4 km resolution configuration of the Regional Ocean Modeling System (ROMS), introduced by Graham et al. [2016]. The model bathymetry and ice shelf depths are gridded from BEDMAP2 [Fretwell et al., 2013] at 4 km resolution. There are 24 vertical levels with increased resolution at the top and bottom. It is forced with 6-hourly wind data and monthly mean climatology for atmospheric temperature, pressure, precipitation, humidity, and cloud cover from the Antarctic Mesoscale Prediction System (AMPS) archived forecasts [Powers et al., 2003]. A dynamic sea ice model [Budgell, 2005] and thermodynamically active ice shelves [Dinniman et al., 2007] are included in the circulation model. Further details of the model can be found in Graham et al. [2016].

The circulation model ran for 7 years, between January 1, 2006 and December 31, 2012. Virtual Lagrangian drifters were released in the model beginning after the first full year of simulation. The particles are advected by the full three-dimensional velocity of the model at every model time step and are also subject to a vertical diffusion component, which was included as a random walk in the vertical direction (Hunter et al., 1993; Visser, 1997). A total of 26,460 drifters were released at 9 depths at 70 locations near the shelf break. A full set of drifters (at each geographic location and depth) was released every two days for a period of one month in January 2007, 2008, and 2009. Simultaneously, and similarly staggered, a total of 12,096 drifters were released at 9 depths at 32 locations within

Palmer Deep alone (Figure 3-1 and Table 3-1). The drifters followed the current field within the model for up to six years, from their release date until December 31, 2012, or whenever they were advected out of the model domain. Each drifter recorded longitude, latitude, temperature, salinity, density, depth, and velocity at one-hour time steps.

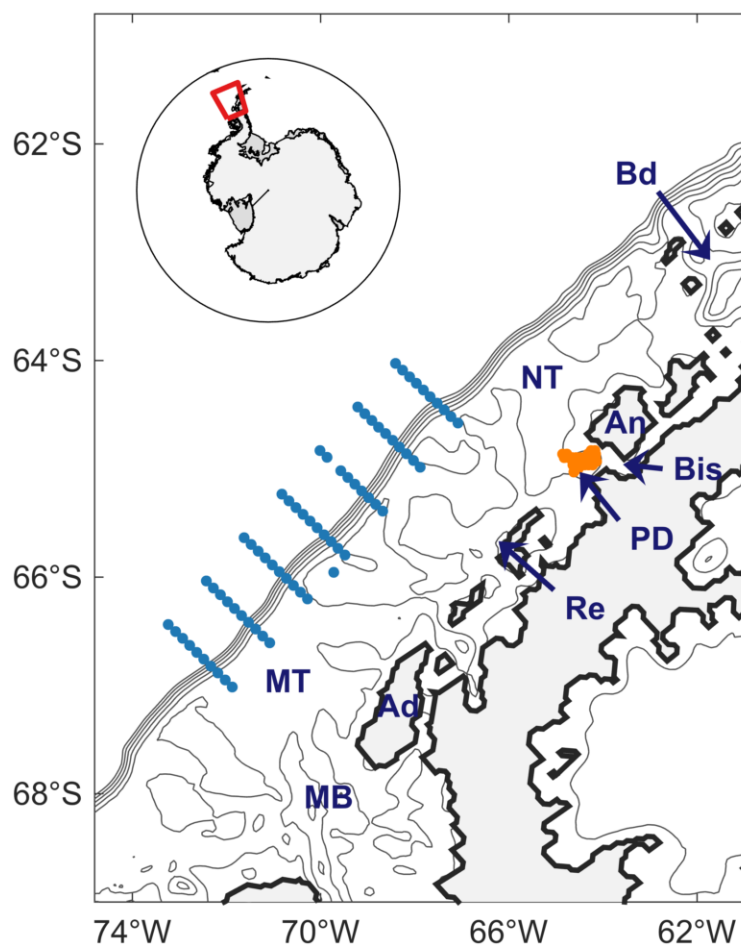


Figure 3-1: Map of study area and locations of drifter release points. Locations of drifters released along the shelf break (blue dots) and within Palmer Deep canyon (orange dots) are indicated. Inset map shows location of study area on the west side of the Antarctic Peninsula. Geographic and bathymetric features are labeled as: An (Anvers Island), Ad (Adelaide Island), Re (Renauld Island), PD (Palmer Deep), Bd (Boyd Strait), Bis (Bismarck Strait), MT (Marguerite Trough), MB (Marguerite Bay), and NT ("northern trough").

Table 3-1: Timing and locations of drifter releases in the model

| | Shelf break | Canyon |
|---------------------------------|---|---|
| Total number of drifters | 26,460 | 12,096 |
| Number of release points | 70 | 32 |
| Release depths (m) | 100, 200, 250, 300, 350, 400, 450, 500, 600 | 100, 200, 300, 400, 500, 600, 800, 1000, 1200 |
| Release dates | 1 January to 27 January, at 2-day intervals | 1 January to 27 January, at 2-day intervals |
| Release years | 2007, 2008, 2009 | 2007, 2008, 2009 |

There are known limitations of this model, but it is expected to do well at simulating the mean trajectories of Lagrangian drifters toward and within Palmer Deep. At 4 km resolution, this model fails to resolve small-scale circulation on the shelf (eddies have been observed with a radius of 3-5 km [e.g. Martinson and McKee, 2012; Moffat et al., 2009]). However, mean pathways of circulation on the shelf are dominated by bathymetry, and are reproduced in this model. This model underestimates the average subpycnocline temperature and heat flux across the shelf break [Graham et al., 2016]. Increasing the resolution to 1.5 km has been shown to more accurately represent these distributions, but the 4 km resolution does a sufficient job at identifying regions of the shelf where warm water intrudes, as confirmed by tagged-seal observations [Graham et al., 2016]. At both 4 km and 1.5 km, the variability in fluxes across the shelf break has also been shown to be similar. Comparisons with gridded ADCP observations from 200 m indicate that a model in this with 4 km resolution region does a good job of describing the circulation on the shelf itself [Dinniman and Klinck, 2004]. The Antarctic Coastal Current, a feature that may extend along the length of the peninsula including along

the west coast of Anvers Island [Moffat *et al.*, 2008], is not well resolved in the model. There is no consistently flowing southward coastal current at Adelaide Island, although the current does appear when local winds are favorable. The model does not include any influence of tides, which have a relatively low range in this area [Klinck, 1995; Oreiro *et al.*, 2014].

3.4 Results

3.4.1 Pathways from the shelf break to Palmer Deep

The majority (71%) of drifters that reached Palmer Deep were released on the shelf itself (shoreward of the 500 m isobaths, Figure 3-2) rather than offshore where unmodified UCDW can always be found within a strong northward-flowing current [Martinson *et al.*, 2008]. Most of the drifters that reached the canyon came from deep waters (> 200 m) just shoreward of the shelf break. In particular, those that reached the canyon within 180 days came from depths around 300 m. Water that originates at this depth along the shelf break is likely to contain UCDW, and the majority of drifters released along the shelf break did initially begin with characteristics defining UCDW (Figure 3-2). Since the model tends to slightly underestimate maximum temperature below the permanent pycnocline [Graham *et al.*, 2016], we use drifters beginning with a temperature above 0°C below a depth of 200 m to represent UCDW.

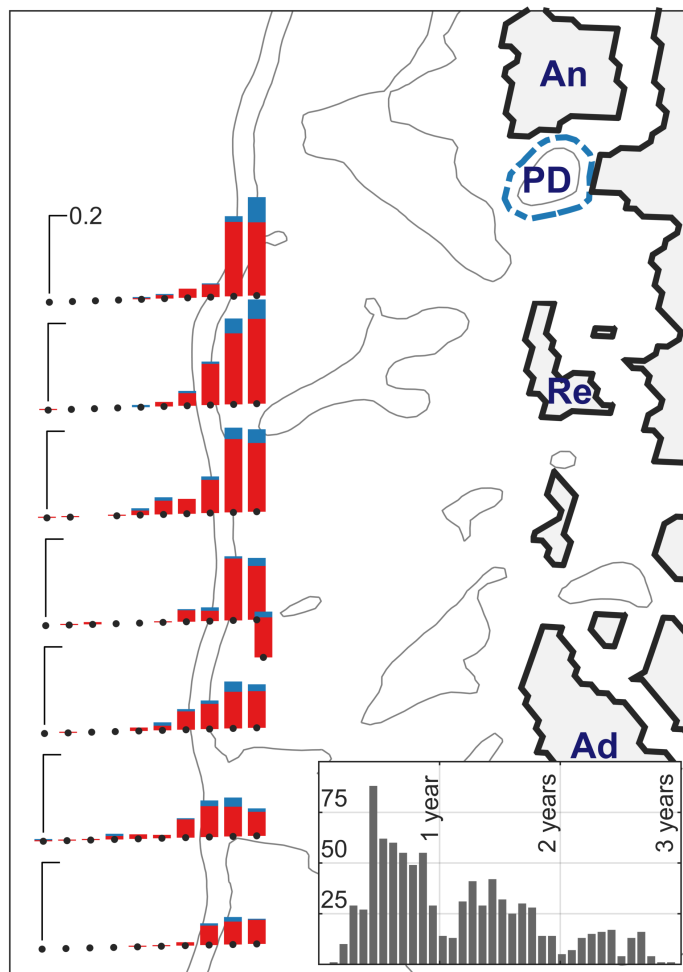


Figure 3-2: Percentages of drifters that reached Palmer Deep. Percentages of drifters released from all depths at each shelf break location that eventually reached Palmer Deep are shown as blue bars at the release sites. Red bars show the subset of drifters that began with characteristics defining UCDW. Bars are placed at drifter release locations (dots) and bar heights are proportional to percentages. Y-axis indicator on shoreward side marks 20% level (20% of drifters released from here reach Palmer Deep). Anvers Island (An), Renauld Island (Re), Adelaide Island (Ad) and Palmer Deep (PD) are labeled (see Figure 3-1). Depth contours are at 500 and 1000 m and Palmer Deep boundary is shown by blue dashed line. Inset plot shows histogram of travel times between release and entry into Palmer Deep. Each bar encompasses 30 days.

The 300 m contour was used to define the boundaries of Palmer Deep (Figure 3-2). This isobath encircles the canyon and opens at the mouth at the southwest corner where the bottom depth deepens to >400 m. The boundary was

connected across this opening by expanding the shape of the 500 m contour outward. The time at which each drifter entered the canyon by crossing the boundary was used as the endpoint from which drifter trajectories were back-calculated. The model domain was divided into 20 km x 20 km grid boxes within which drifters were counted. Figure 3-3 and Figure 3-4 show the number of drifters that passed through each grid box 14 and 30 days prior to entering the canyon, respectively. The majority of drifters enter the canyon from the north. Particularly in the 200-400 m range, they hug the west coast of Anvers Island, first traveling southward and then turning eastward into Palmer Deep. Paths of individual drifters indicate that the northern trough funnels water toward Palmer Deep on its northern side and moves water out toward the shelf break on its southern side (Figure 3-5).

Drifters entering Palmer Deep from their initial starting positions at the shelf break took one of four primary pathways. Tracks of the 90 days prior to canyon entry illustrate three of these pathways (Figure 3-5). In the first, drifters already on the shelf or on the slope made a cyclonic loop through the northern trough, traveling offshore along its northern wall. The second pathway also looped around the northern trough, but drifters continued northward to Boyd Strait before coming back toward Palmer Deep. In the third pathway, drifters remained on the shelf slope, traveling northward, until they reached Boyd Strait and were pulled into the shelf interior there. A fourth set of drifters approached Palmer Deep from the south and entered the canyon before ever reaching the latitude of the northern trough.

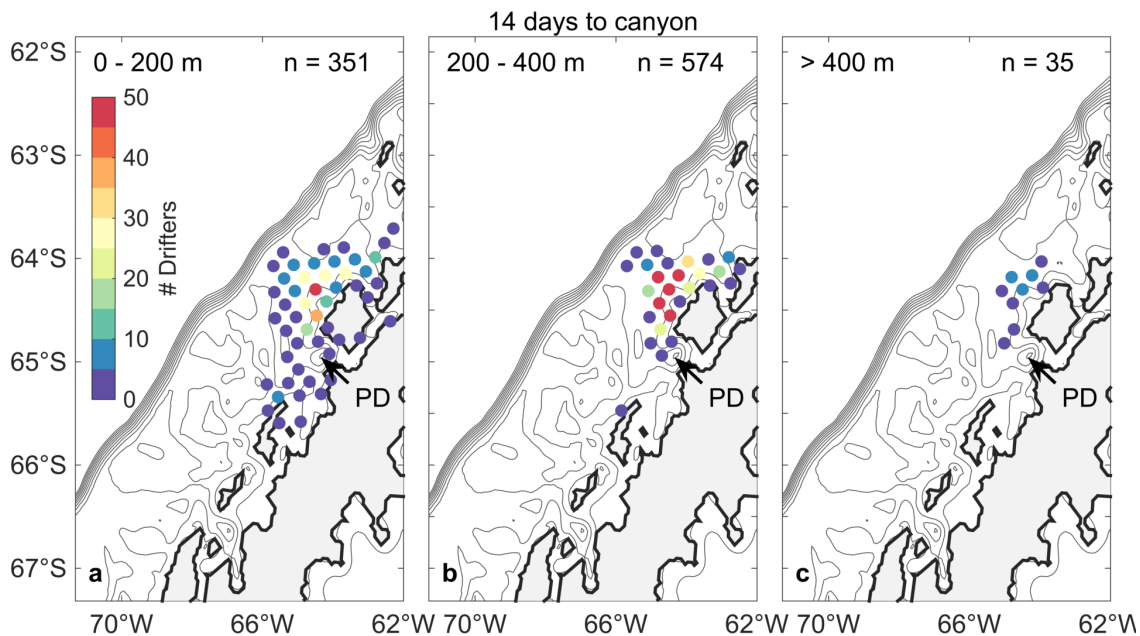


Figure 3-3: Counts of drifters within 20 x 20 km grid boxes 14 days before each entered the canyon.
Data shown are only from drifters released from shelf break. Drifters entering the canyon at three depth ranges are shown: a) 0-200 m, b) 200-400 m, and c) >400 m.

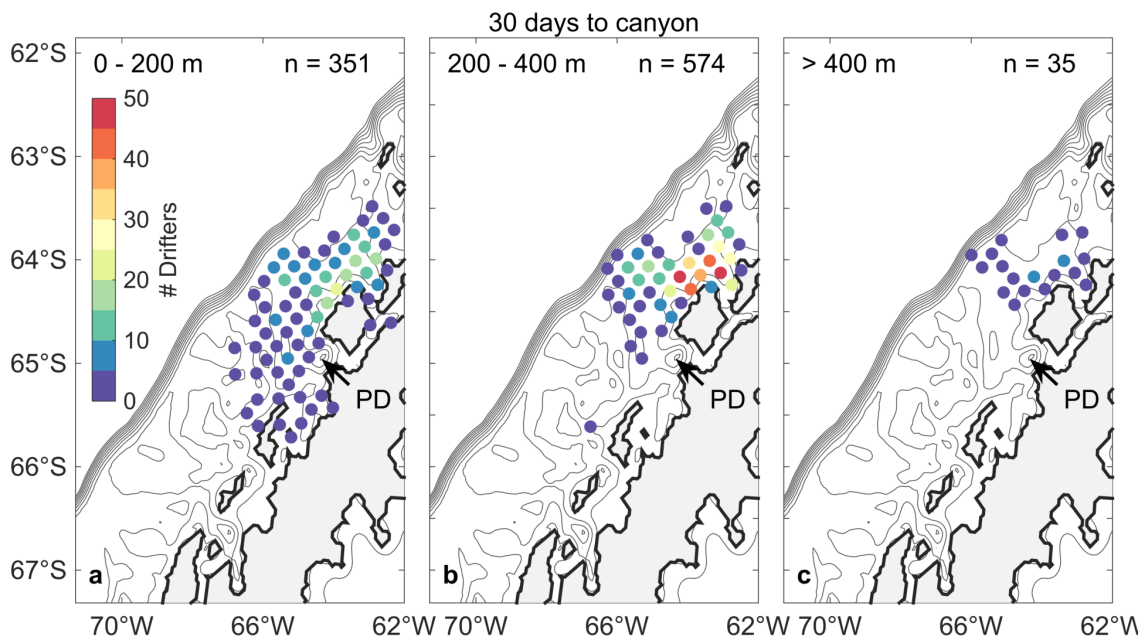


Figure 3-4: Counts of drifters within 20 x 20 km grid boxes 30 days before each entered the canyon.
Data shown are only from drifters released from shelf break. Drifters entering the canyon at three depth ranges are shown: a) 0-200 m, b) 200-400 m, and c) >400 m.

These drifters were already well on the shelf 90 days prior to reaching Palmer Deep and were mostly confined to the upper 200 m of the water column, where the signal of UCDW is not strong.

Total travel times to the canyon varied widely, from 54 days to nearly 6 years with a median of 396 days. In many cases, paths shown in Figure 3-5 represent only the end of long trajectories that took drifters around other trough-contained cyclonic gyres on the shelf. Drifters that began as UCDW arrived periodically to Palmer Deep, with more reaching the canyon 6 months, 18 months, and 30 months

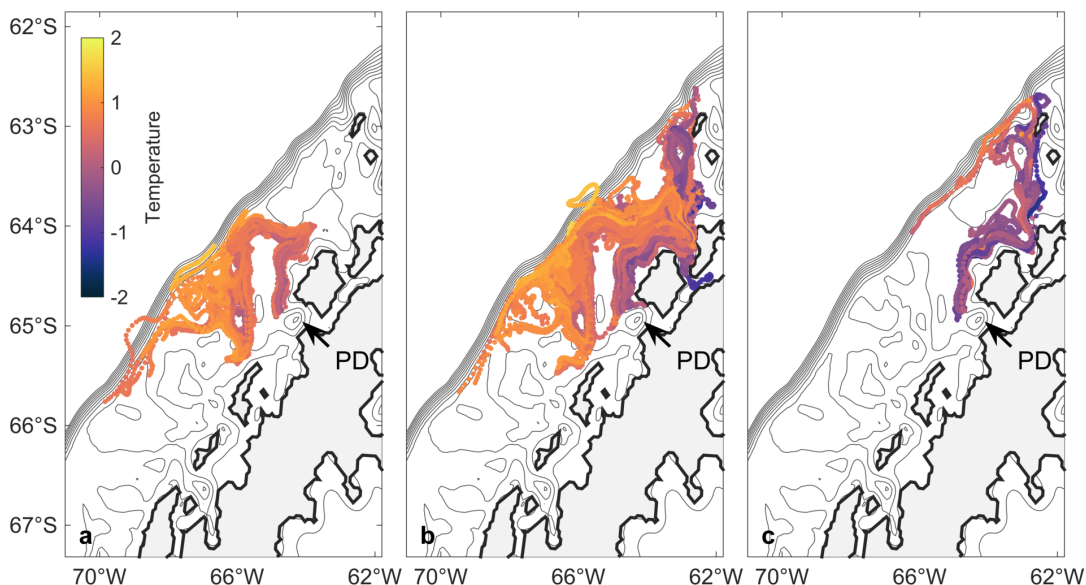


Figure 3-5: Examples of drifter approaches to Palmer Deep. All paths are between 200 and 400 m and show the 90 days prior to entering Palmer Deep. Temperature along paths is indicated by color. Subplots show three of the four primary approaches to Palmer Deep: a) via the cyclonic circulation of the northern trough, b) via extended circulation through the northern trough and Boyd Strait, and c) entering the shelf interior through Boyd Strait. The fourth common approach, from south of Palmer Deep, is not shown because most of the 90-day approaches occurred at depths shallower than 200 m.

from release compared to one year, 2 years, and 3 years, respectively (Figure 3-2). Since all drifters were released during the month of January, this implies that more drifters entered the canyon each year during July than January.

3.4.2 Modification of water properties

Modified UCDW was found to enter the canyon during all seasons at depths below ~150 m. Temperature and salinity of drifters entering the canyon decreased from their initial starting values along the shelf break (Figure 3-6). The temperature of drifters entering the canyon depended strongly on the depth at which they entered and the northernmost position they had reached on the shelf. Drifters that had traveled further north on the shelf were cooler when they entered the canyon. Among drifters that entered the canyon below 200 m (approximating the depth of

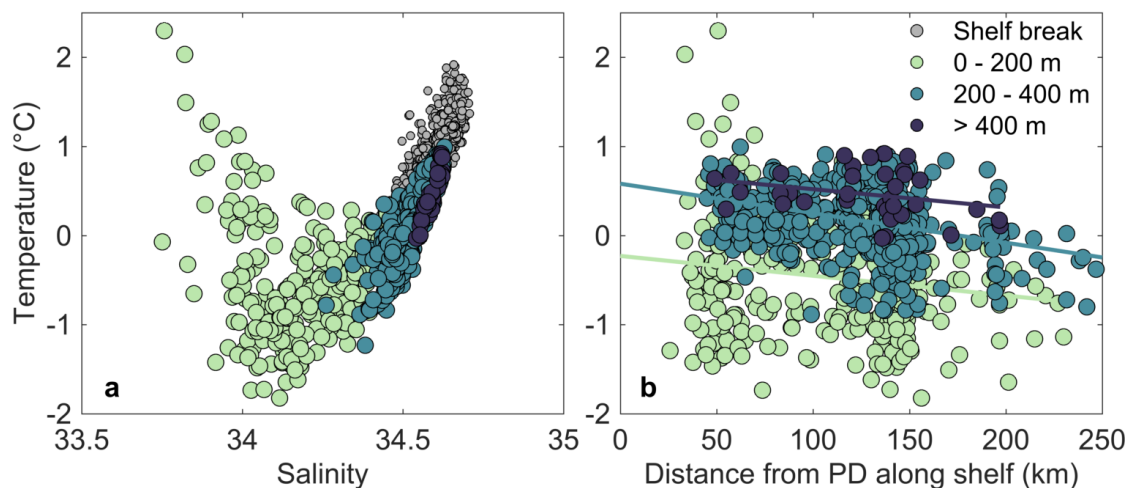


Figure 3-6: Changes in drifter temperature and salinity. a) Temperature-salinity (TS) plot of initial values of drifters released on the shelf break (grey dots) and their values upon entering Palmer Deep (colored dots). b) Temperature of drifters entering Palmer Deep vs. the farthest distance each drifter traveled along the shelf break (0 km is distance along shelf where a perpendicular drawn to the shelf break crosses the center of Palmer Deep. Boyd Strait sits at about 150 km).

the permanent pycnocline), temperatures of drifters that had entered Boyd Strait cooled the most (Figure 3-5).

A significant number of drifters completely circled the northern trough at least once, and often several times before entering the canyon (not shown). Retention within this trough increased the travel time to Palmer Deep but the distribution of water properties entering the canyon was not significantly different between drifters that were trapped in the trough and drifters that passed straight through it. The depth of canyon entry and the northern limit of a drifter's pathway before entering the canyon controlled its water properties at the time of entry. Some of the drifters that originated as UCDW at the shelf break entered the canyon as Antarctic Surface Water, but these had traveled for over a year.

3.4.3 Canyon entry and exit

The 300 m isobath canyon boundary was divided into four "gates" approximately 30 km wide. The number of drifters that entered the canyon through each of the gates varied with depth and season (Figure 3-7 and Figure 3-8). The largest inflow and outflow was through the west-facing mouth of the canyon, at depths between 200 and 400 m. There was strong inflow through the northern side of the canyon and strong outflow through the southern side. Water exchange between Palmer Deep and Bismarck Strait was concentrated at shallower depths because the water depth there is shallower than 300 m.

Through Bismarck Strait, the inflow and outflow were strongest during summer, and generally weak during other seasons. Outflow through the southern

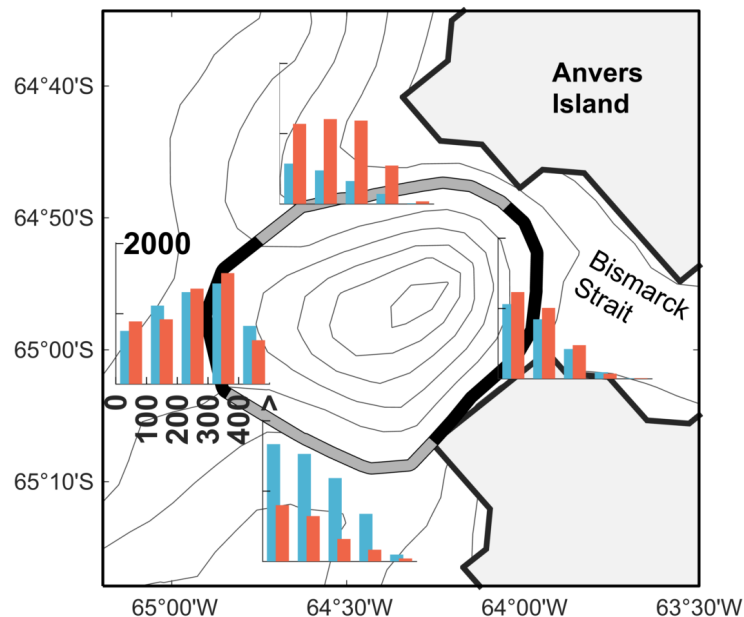


Figure 3-7: Canyon entry and exit by depth.

Histograms of depths at which drifters entered (red) and exited (blue) the canyon through each gate. Axes shown on the western gate are the same for all others. The y-axis shows the number of drifters that passed through in each depth bin. The x-axis shows depth bins of 0-100, 100-200, 200-300, 300-400, and >400 m. Data plotted here come from drifters that originated along the shelf break and as well as those that started in the canyon, exited, and eventually re-entered.

boundary was also strongest during summer and fall. Flow into the northern

boundary and out of the western canyon mouth were both slightly elevated during

fall and winter.

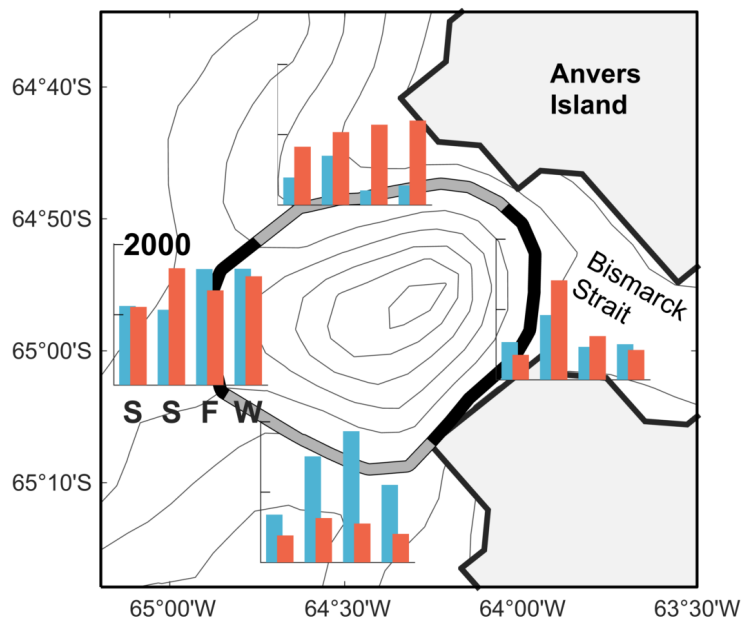


Figure 3-8: Canyon entry and exit by season.

Histograms of depths at which drifters entered (red) and exited (blue) the canyon through each gate. Axes shown on the western gate are the same for all others. The y-axis shows the number of drifters that passed through during each season (x-axis: S=spring, S=summer, F=fall, W=winter). Data plotted here come from drifters that originated along the shelf break and as well as those that started in the canyon, exited, and eventually re-entered.

3.4.4 Retention time in Palmer Deep

Retention time in Palmer Deep was calculated two different ways depending on whether drifters were initially released inside or outside the canyon. Following Piñones et al. [2011], retention time was estimated as the time it took for the fraction of drifters released from various depth ranges within the canyon to decrease to 0.3679 (the e-folding time scale). First, the fraction of particles that remained in the canyon from each depth bin was used to determine the decay constant, λ , to create an exponential fit to the data:

$$f(t) = f_0 e^{-\lambda t}, \quad (3-1)$$

where t is the time in days, f_0 is the initial fraction of particles at $t=0$, and f is the fraction of particles remaining at each time step. The e-folding time scale was then calculated for each depth range. These residence times are shown in Figure 3-9 along with those calculated using the second method.

In method 2, drifters entering the canyon were tracked from their time of entry into the canyon until their subsequent exit. The average retention time of all drifters that entered at each depth range and during each season is shown in Figure 3-9. Retention times, calculated with either method, increased with depth of entry

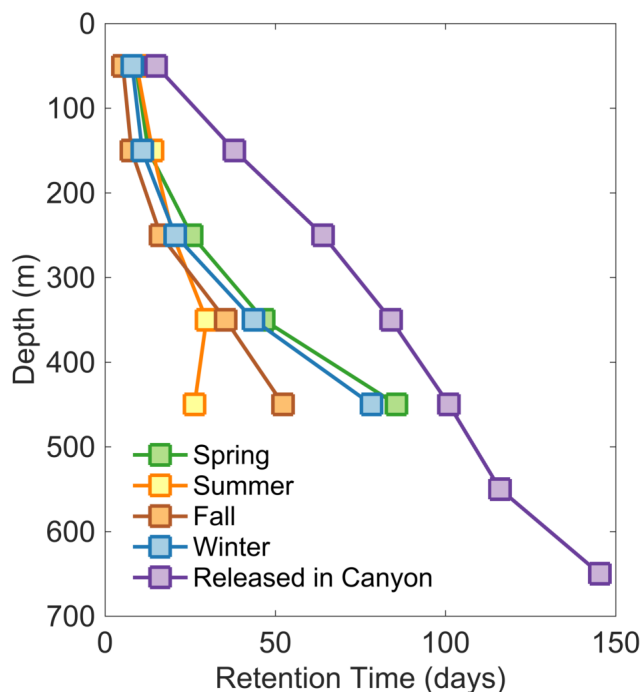


Figure 3-9: Retention time in Palmer Deep.

Average retention time of drifters that entered Palmer Deep within different depth ranges during different seasons (labeled Spring, Summer, Fall, Winter, method 2), and the retention time of drifters released in Palmer Deep at different depths (all during January, method 1). For drifters tracked from entry to exit, retention times are averaged for 100-m depth bins between 0 and 400 m and for all depths below 400 m. For drifters released in the canyon, retention times are averaged for 100-m depth bins between 0 and 600 m and for all depths below 600 m.

or depth of release within the canyon. Below 200 m, retention times were longer for drifters entering the canyon during winter and spring than for those that entered during summer and fall. Retention time estimated using method 1 was higher than estimates using method 2 for all depths, but it should be noted that all drifter releases in the canyon were done in spring.

3.5 Discussion

3.5.1 Entry onto the WAP shelf

Dinniman and Klinck [2004] showed that intrusions of UCDW into the center of the WAP shelf require two mechanisms. First, UCDW must already be on the shelf, having crossed the shelf break at locations where the bathymetry curves shoreward and the flow follows it onto the shelf. Second, once on the shelf, UCDW is pulled into the interior by following the general shelf circulation. Prézelin et al. [2004] identified two areas in this region of the WAP where UCDW enters the shelf: Marguerite Trough and what we've identified here as "the northern trough".

Our results indicate that UCDW is pulled into the shelf interior at the two troughs indicated by Prézelin et al. [2004] as well as through the trough that crosses the shelf break offshore of Renauld Island (Figure 3-5 a and b). Cyclonic gyres associated with each of these bathymetric features move water toward the coast on their north/east sides and away from the coast on the south/west sides [Dinniman and Klinck, 2004]. Many of the drifters that reached Palmer Deep completed a full cyclonic loop through at least one of these troughs on their way to the canyon.

Very few of the drifters that were released off the shelf made it to Palmer Deep during the entire six-year model run. Instead, they were carried northeastward and out of the model domain. Nearly all of the drifters that entered Palmer Deep were pulled into the shelf interior from initial positions at the shelf edge where they were flowing northward. In their 4 km model of the WAP, Graham et al. [2016] found that, north of Marguerite Trough, the peak northward current velocity was centered at the ~500 m isobath. Of the drifters released along the shelf break here, 14% of those released shoreward of the 500 m isobaths reached Palmer Deep while less than 2% of those released between the 500 and 1000 m isobaths reached the canyon.

This suggests that most of the mUCDW entering Palmer Deep first crosses the shelf break farther south than the shelf release points, which has been previously suggested by analysis of available hydrographic data [*Martinson et al.*, 2008]. The water mass is significantly modified by the time it reaches the latitude of Palmer Deep because it has spent a long time traveling at the edge of the shelf where it has the opportunity to mix with cooler water masses that are confined to the shelf. Observations and model results have shown that temperatures in the northern part of the WAP are cooler than those south of Adelaide Island. While temperatures off the shelf are consistently high, the lack of a prominent shelf-crossing location in the north prevents this water from ever reaching the northern WAP. The water that does enter the northern WAP has traveled a long distance from its source, losing heat along the way.

3.5.2 Interaction with the Antarctic Coastal Current

Drifters moving toward Palmer Deep at depths below the permanent pycnocline underwent the most rapid decline in temperature in Boyd Strait and along the west coast of Anvers Island. The Antarctic Coastal Current, a nearly ubiquitous current around the continent, carries relatively cold water from the Weddell Sea around the tip of the peninsula and westward through Bransfield Strait [Heywood *et al.*, 2004]. There is evidence from observations [Savidge and Amft, 2009] and modeled drifters [Matano *et al.*, 2002] that it then crosses over toward the South Shetland Islands and retroflects back out through Bransfield Strait on its eastern side. Drifters that reached as far northeast as the South Shetland Islands reached significantly cooler temperatures than those that remained in the cyclonic circulation of the northern canyon (Figure 3-5 and Figure 3-6).

Proximity to the cold Weddell-sourced water in the Bransfield would allow mixing and modification of the warmer WAP water much more quickly than a circulation pathway of equal distance that did not reach as far to the east. This is likely to be a significant factor controlling the amount of heat that reaches Palmer Deep.

3.5.3 Factors controlling retention time in Palmer Deep

At typical sub-pycnocline depths where mUCDW lies, retention time in Palmer Deep is comparable to the retention time in Laubeuf Fjord [Piñones *et al.*, 2011], a biological hotspot south of Adelaide Island with high densities of copepods, krill [Lawson *et al.*, 2004; Zhou *et al.*, 2004; Ashjian *et al.*, 2008], and pelagic fish

[Donnelly and Torres, 2008]. This retention of nutrient-rich water is important for supporting the productive ecosystem surrounding Palmer Deep.

Retention time in the canyon increases with depth during all seasons and is particularly long during winter and spring (Figure 3-9). Entry into the canyon is also elevated during winter (Figure 3-2) through the northern and western gates. These are the most common entryways used by drifters coming from the shelf (Figure 3-8). During winter, the permanent pycnocline is marked by the bottom of the Winter Water, formed by the cooling of the surface and the formation of sea ice. This boundary is strong throughout the winter and weakens during summer as the surface water is heated and the Winter Water layer begins to erode from warmer water masses both above and below it. During winter, then, water that enters the canyon below this barrier is more likely to be retained for a longer period of time.

Outflow through the southern gate is elevated during summer/fall and at shallow depths. Spring and summertime observations in the canyon have shown that water temperatures in the upper 100 m are cooler in the north and warmer in the south due to upwelling of mUCDW [Carvalho *et al.*, 2016]. This exiting water would be a mix of the shallower water flowing in from the northern gate, which is likely to have been cooled by interactions with more northern water massed before entering the region, and deeper warm water entering through the western gate.

The Antarctic Peninsula Coastal Current is a geostrophically-balanced southward flowing current that runs along the west coast of Adelaide Island and is thought to begin somewhere along or near the coast of Anvers Island [Moffat *et al.*, 2008; Savidge and Amft, 2009]. The clockwise pathways within the northern trough

and toward Boyd Strait may initialize the northern branch of the APCC along Anvers Island. The result that drifters enter the canyon more frequently during winter than summer is consistent with the observation that the northern branch of the APCC is stronger during the winter [*Savidge and Amft, 2009*].

3.5.4 Impact of increased model resolution

In a region where currents are strongly controlled by the topography over which they flow, we expect that repeating this study with increased model resolution would affect the total heat transport to Palmer Deep, but that the seasonal variability in transport and the major transport pathways would be largely unchanged. Eddies are known to be a significant source of heat to the WAP [*Moffat et al., 2009; Martinson and McKee, 2012; St-Laurent et al., 2013; Couto et al., 2017*], and the resolution of this model was insufficient to resolve most mesoscale eddies in the region. Additionally, water that is moving northward along the shelf break is pulled into the canyon interior and deep bathymetric features, so increasing the resolution of the bathymetry may reveal more common entry pathways. Indeed, in their comparison between a 4 km and 1.5 km model of the WAP, Graham et al. [2016] found that the higher-resolution model had increased heat transport due to increased eddy activity, and indicated a location for UCDW intrusion between Marguerite Trough and the northern trough that is not apparent at lower model resolution. Patterns of variability in heat transport, however, were similar between the models. This comparison gives us confidence that the pathways for transport of

UCDW to Palmer Deep that we have described here would be consistent with increased resolution.

3.6 Conclusions

Drifters advected in a 4 km resolution model of the WAP revealed a complicated set of pathways to Palmer Deep. The drifters were initialized just north of the opening to Marguerite Trough both on the shelf edge and off the shelf in the open ocean. Very few of the open ocean drifters made it to Palmer Deep suggesting that the mUCDW that reaches this canyon crosses the shelf break somewhere south of Marguerite Trough. The mUCDW that feeds both Marguerite Bay and Palmer Deep is likely to cross the shelf break at the same location. The water that floods the northern part of the WAP is cooler because it has spent more time traveling on the shelf or at the shelf edge mixing with cooler overlying water masses.

Drifters that reached Palmer Deep were pulled into one of several shelf-incising troughs and were advected in their cyclonic circulation. Drifters entered the canyon more commonly during winter than summer and were retained for longer periods of time at depth when they entered during winter. Within three months prior to entering Palmer Deep, most drifters were in the northern trough or had been advected as far north as Boyd Strait. The farther north a drifter had traveled during these three months, the cooler it could be expected to be when it reached the canyon.

As the WAP climate changes, winds are expected to shift [*Thompson and Solomon, 2002*], which may alter the locations and frequency of UCDW intrusion

onto the WAP as well as the extent to which the Antarctic Coastal Current influences the WAP shelf. These interactions between water masses are important to understand because they affect the properties of the water fueling an important Antarctic coastal ecosystem. The results presented here improve our baseline understanding of the water masses that fuel Palmer Deep to which future changes can be compared.

4 Tidal and wind-driven controls on heat flux at the head of Palmer Deep Canyon

4.1 Introduction

The continental shelf west of the Antarctic Peninsula (WAP) has undergone rapid environmental change in recent years. Heat flux from the ocean to the atmosphere is an important contributor to the significant atmospheric warming over the WAP shelf, particularly during winter [Vaughan, 2005; Martinson and McKee, 2012; Turner *et al.*, 2012]. The largest source of oceanic heat to the region is Upper Circumpolar Deep Water (UCDW), which originates offshore within the eastward flowing Antarctic Circumpolar Current (ACC) [Hofmann *et al.*, 1996]. Increased delivery of UCDW onto the shelf has led to an increase in the mean subpycnocline water temperature on the WAP shelf [Martinson *et al.*, 2008], making more heat available to the underside of glacial ice shelves [Martinson and McKee, 2012]. Understanding the processes that transport this water mass from its offshore source onto the continental shelf and into the coastal canyons and fjords is an active area of research. Topographic steering, Ekman-induced upwelling, and eddy shedding have all been identified as important mechanisms acting at the shelf break [Moffat *et al.*, 2009; Klinck and Dinniman, 2010; Martinson and McKee, 2012]. Measurements of heat flux closer to the coast, however, remain scarce. Warm modified UCDW (mUCDW) is found across all areas of the shelf, even in shallow nearshore regions [Smith *et al.*, 1995a], so it is critical to understand the transport and transformation processes that modify this important water mass as it moves

across the shelf to the coast. A comprehensive understanding of these processes is necessary to better constrain the heat budget across the shelf.

UCDW preferentially moves onto the shelf at subsurface troughs and continues along them toward the coast [*Prézelin et al., 2004; Moffat et al., 2009; Klinck and Dinniman, 2010; Martinson and McKee, 2012*]. Subpycnocline waters across the WAP are flooded with mUCDW, but certain areas of the shelf retain the water mass for longer periods of time. This occurs especially in coastal canyons and the retention is thought to contribute to the capacity of these canyons to support productive biological systems [*Allen et al., 2001; Piñones et al., 2011*]. Excess heat and nutrients are retained at depth and are made available to support primary producers when they are upwelled into the surface waters. High retention times also keep zooplankton like krill from being advected out of the area as they mature [*Piñones et al., 2011*].

Palmer Deep is a deep coastal canyon in the northern part of the WAP considered to be one of the region's biological hotspots. It lies a few kilometers southwest of Anvers Island, where the United States research base Palmer Station is located (Figure 4-2). The islands surrounding Palmer Deep are important nesting grounds for penguins and the canyon is associated with a high level of biological activity [*Ducklow et al., 2013; Oliver et al., 2013; Schofield et al., 2013*]. UCDW retained within the canyon is thought to create a suitable habitat for primary producers by providing an abundance of nutrients and by melting sea ice in the spring to create areas of open water and a more stratified water column [*Kavanaugh et al., 2015*]. Upwelling of UCDW has been observed at the head of Palmer Deep and

has been linked to increased concentrations of phytoplankton biomass [*Schofield et al., 2013; Carvalho et al., 2016*].

The Palmer Station Long Term Ecological Research project (LTER) has been measuring water properties in the upper 80-100 m of the water column at a location approximately 4 km from Palmer Station for the past 25 years [*Smith et al., 1995b; Ducklow et al., 2007*]. Station E sits at the head of Palmer Deep on a ledge where the water depth is approximately 150 m but quickly drops off to >600 m. Hydrographic measurements at Station E reveal that the subpycnocline water is oceanic in origin, and it has been hypothesized that Palmer Deep acts as a conduit for modified UCDW to the nearshore [*Schofield et al., 2013; Carvalho et al., 2016*]. The seasonal cycle of primary productivity [*Schofield et al., 2017a*] and bacterial productivity [*Ducklow et al., 2012*] have been monitored at this site for decades and put in the context of nutrient and light supply, but current speeds and heat transport, which significantly affect the physical environment, have not been monitored.

Tidal and wind-driven circulation in the canyon can influence patterns of nutrient availability and local concentrations of zooplankton [*Bernard and Steinberg, 2013*]. Circulation within the canyon is thought to create episodic convergent zones where krill accumulate, providing high densities of prey for penguins, seals, and whales [*Kohut et al., 2016*]. In particular, tides are known to affect the distance Adélie penguins travel during their foraging trips [*Oliver et al., 2013*]. The Palmer area experiences a mixed tide in which diurnal and semidiurnal tides alternate every 5-10 days, with short transition periods between. Penguins

travel greater distances during periods of semidiurnal tides than during diurnal periods [*Oliver et al.*, 2013].

Wind stress also affects local circulation and mixing of the ocean surface layer. Large krill aggregations in the shallow areas shoreward of the canyon head are most common during diurnal tides and periods when the winds blow primarily from the west, which would transport water from the center of Palmer Deep [*Bernard et al.*, 2017].

The aim of this study is to quantify the heat flux near the terminus of the UCDW transport pathway across the shelf and to assess the influence of tides, winds, and sea ice on this transport. We focus on a nearshore location associated with a subsurface canyon on the WAP shelf. For a period of 75 days during the austral spring and summer of 2015-16, a subsurface mooring was deployed at Station E. Rates of bottom heat flux measured at this location represent the end member of UCDW transport onto the WAP shelf, having been modified significantly by the time it reaches the site. This study will provide some physical context for the biological parameters routinely measured at Station E.

4.2 Background on regional circulation

Measurements of water mass properties, primary production, and bacterial production at Station E have been made regularly since 1990, representing one of the longest time series in Antarctica [*Ducklow et al.*, 2012]. However, measurements of ocean currents at this site are made infrequently, so the effect of circulation on these properties is poorly understood. Until the last decade, most of what was

known of circulation on the WAP was based on hydrographic data and dynamic height estimates. More recently, Savidge and Amft [2009] compiled 6 years of Acoustic Doppler Current Profiler observations from cruises on the WAP aboard the R/V *Gould* and R/V *Palmer* to describe circulation more in detail. The general circulation described by hydrography was verified and some additional insights were added. Here, we provide an overview of the general circulation characteristics relevant to the area surrounding Palmer Deep and the head of the canyon itself.

The WAP shelf is characterized by cyclonic flow with the northeastward-flowing limb along the shelf edge, just shoreward of where the northeastward-flowing Antarctic Circumpolar Current (ACC) abuts the shelf edge [Hofmann *et al.*, 1996]. The nearshore southwestward flow is driven by downwelling-favorable winds [Hofmann *et al.*, 1996], which are dominant throughout the year [Van Loon, 1967]. There is seasonality in the nearshore buoyancy forcing [Stammerjohn and Smith, 1996], caused by freshwater input at the surface, which leads to seasonality in the nearshore limb of the cyclonic circulation [Moffat *et al.*, 2008; Savidge and Amft, 2009].

A surface-intensified southeastward flow called the Antarctic Peninsula Coastal Current [Moffat *et al.*, 2008] exists just seaward of the nearshore islands along the WAP (Anvers, Adelaide, Alexander), and while it has been observed everywhere along the nearshore islands from Anvers to Alexander, it is still not clear whether the current is continuous [Moffat *et al.*, 2008; Savidge and Amft, 2009]. Off of Anvers Island, the flow is stronger in the winter and off Adelaide Island, the flow is stronger in the summer. It is unknown whether the flow off

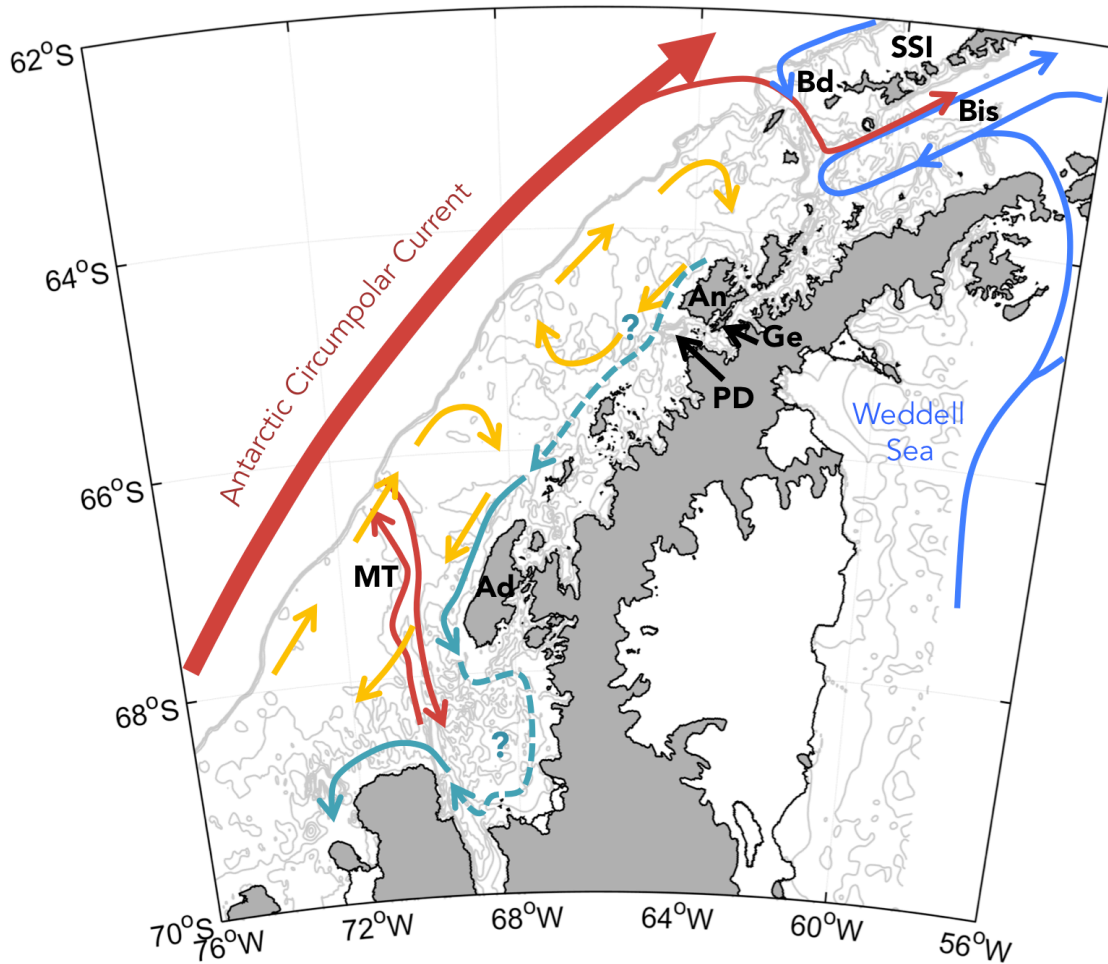


Figure 4-1 Map of WAP circulation

Known circulation patterns, drawn from Moffat et al. [2008] and Savidge and Amft [2009]. Depth contours are drawn at 250 m intervals from 0 to 1000 m. The Antarctic Circumpolar Current and the deep transport of UCDW through Marguerite Trough are shown in red. Yellow arrows indicated surface circulation. Teal arrows indicate the Antarctic Peninsula Coastal Current with solid lines showing known paths and dashed lines showing proposed paths. Blue arrows indicate flow from the Weddell Sea as part of the Antarctic Coastal Current and the Polar Slope Current. Geographic and bathymetric features are labeled as: SSI (South Shetland Islands), Bis (Bismarck Strait), Bd (Boyd Strait), An (Anvers Island), Ge (Gerlache Strait), PD (Palmer Deep), and MT (Marguerite Trough).

Adelaide Island is fed by input from the north, or is supplied from Marguerite

Trough, through which a cross-shelf flow exists [Savidge and Amft, 2009]. The shelf circulation is broken up into at least two sub-gyres that are at least partially driven

by bathymetry. Transport between the northeastward and southwestward limbs of the cyclonic circulation is accomplished through a few shelf-incising troughs [Hofmann *et al.*, 1996].

Cyclonic circulation also exists in the northern part of the shelf, in Bransfield Strait, which remains mostly separated from the rest of the WAP shelf, although circulation above 500 m may be important in transporting WAP shelf water into the Bransfield [Hofmann *et al.*, 1996]. The Antarctic Coastal Current flows from the Weddell Sea, around the tip of the peninsula, and westward across Bransfield Strait. When it reaches Boyd Strait, it retroflects back toward the north [Savidge and Amft, 2009]. Therefore, there is little mixing between Bransfield Strait and the rest of the shelf [Moffat *et al.*, 2008]. On the seaward side of the South Shetland Islands, the Polar Slope Current flows southward and then turns into Boyd Strait. Boyd Strait also receives some input from the northeastward limb of the general WAP circulation along the shelf slope. This flow turns clockwise into the strait as a “meander” that continues flowing eastward along the south side of the South Shetland Islands [Hofmann *et al.*, 1996].

While the general circulation of the WAP shelf is fairly well understood, there are still important gaps in our knowledge. For example, transport to the nearshore areas south of Anvers Island, where myriad biological factors have been measured for decades, are not well described. Here we provide a detailed analysis of water column velocities and bottom heat flux at the terminus of an important UCDW pathway to the coast. These observations are assessed in the larger context of the general circulation on the WAP shelf.

4.3 Observations

4.3.1 Acoustic Doppler Current Profiler (ADCP) and Conductivity-Temperature-Depth (CTD) data

A subsurface mooring equipped with an upward-looking 300 kHz Acoustic Doppler Current Profiler (ADCP) and a Conductivity Temperature Depth sensor (CTD) was deployed at a depth of 147 m at $64^{\circ} 48.9'S$, $64^{\circ} 02.4'W$ between November 25, 2015 and February 9, 2016 (Figure 4-2). The ADCP measured current

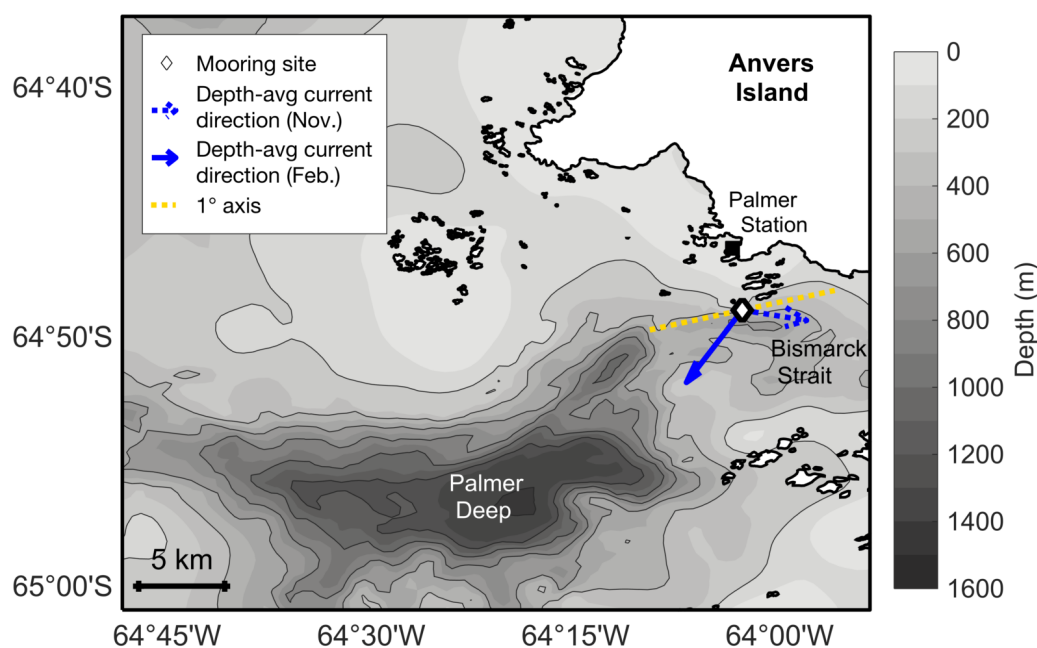


Figure 4-2: Map of mooring location.

The mooring deployment site is indicated by the diamond. The dashed yellow line shows the principle axis of motion for depth-averaged currents throughout the mooring period. The dashed blue arrow indicates the direction of depth-averaged currents during the first two weeks of deployment and the solid blue arrow indicates the direction of depth-averaged currents during the final two weeks of deployment. The lengths of the blue arrows conserve the relative magnitude of the depth-averaged currents in November and February, but their lengths compared to the map scale are meaningless.

velocity in 2 m bins from a depth of approximately 143 m to 20 m below the surface while the CTD provided temperature and salinity data at 146 m.

Every ten minutes, measurements of bottom temperature and current velocity throughout the water column were recorded at one-second intervals for a period of one minute. All measurements throughout this period were averaged to obtain one value every ten minutes.

Temperature and salinity profiles were also taken approximately twice a week throughout the upper 80 m of the water column at the mooring site as part of the Palmer Station Long Term Ecological Research project [Smith *et al.*, 1995b; Ducklow *et al.*, 2013]. A linear trend was removed from the temperature data in order to focus on the role that winds and tides have on heat flux, without the effect of seasonal warming. Detrended temperatures were adjusted by the mean value so that the detrended temperature series maintained the same mean as the original series (Figure 4-4). Total integrated heat flux throughout the duration of the deployment did not differ significantly ($\sim 1\%$) whether the original or detided temperature data were used.

Current velocity, temperature, and salinity time series were smoothed using a one-hour running mean filter and then decomposed into their low- and high-frequency components using a 36-hour Lanczos filter. The high-frequency data represent tidal and inertial oscillations and the low-frequency data reflect the response of sub-tidal oscillations and represent time-averaged flow characteristics on approximately daily timescales.

4.3.2 Wind

Palmer Station, located 4 km from the mooring location maintains an archive of meteorological observations. Wind speed and direction are measured at a height of 10 m at 2-minute intervals. These data were interpolated to the same 10-minute intervals of the ADCP and CTD data and were filtered into low-frequency and high-frequency components using the same 36-hour Lanczos filter.

4.3.3 Sea ice

Daily sea ice concentration measurements were taken from the AMSR2 3.125 km archive [Beitsch *et al.*, 2013]. To estimate the daily sea ice concentration at the mooring site, we averaged the concentrations measured at the four grid cells nearest the mooring.

4.4 Results

4.4.1 Seasonal and physical context

A near-bottom current meter and CTD were deployed at Station E from late spring to mid-summer of 2015-2016. A continuous record of water temperature at 6 m at Palmer Station, approximately 4 km from the mooring site, provides seasonal context for the deployment. These data reveal a seasonal trend in which water temperatures cool to freezing during winter when sea ice is present, warm to approximately 1°C in the spring and summer, and begin to cool again in fall (Figure 4-3). Observations at the mooring site were made during the warmest part of the year, including the warming period, but ending before the cooling period began.

Temperatures in the upper 80 m of the water column, measured bi-weekly from a lowered CTD, increased at rates of $0.025 - 0.040 \text{ } ^\circ\text{C day}^{-1}$ until January 20th and slowed to warming rates less than $0.01 \text{ } ^\circ\text{C day}^{-1}$ after that. Bottom temperatures, measured by the CTD on the mooring, continued to rise throughout the deployment at a rate of $0.010\text{-}0.015 \text{ } ^\circ\text{C day}^{-1}$, although it should be noted that the mooring was recovered approximately one month before bi-weekly water column sampling ended.

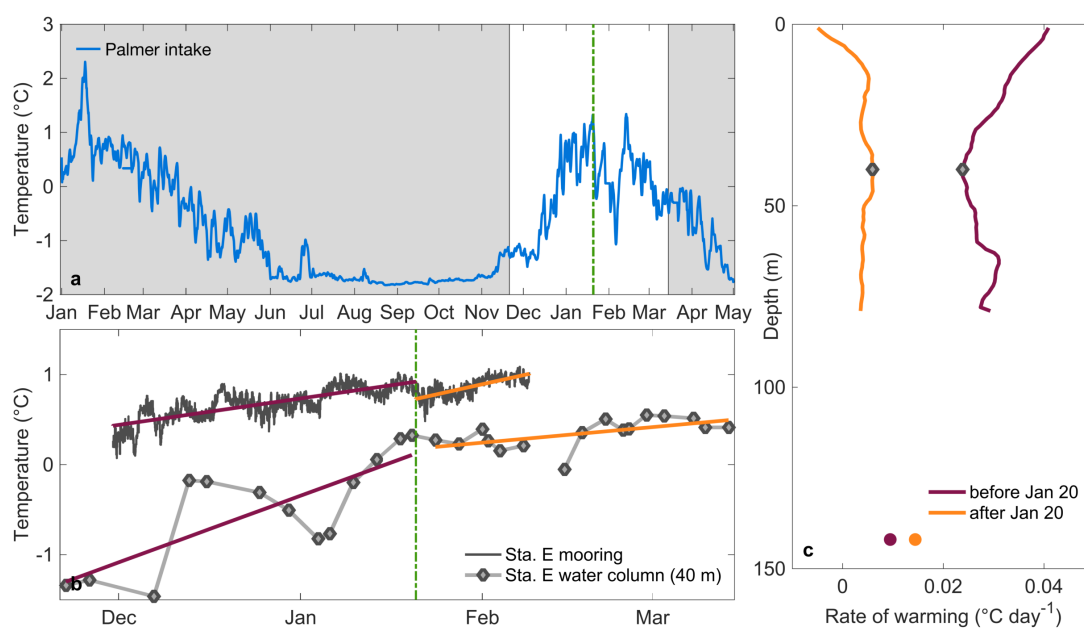


Figure 4-3: Temperature records at Palmer Station and Station E.

a) Palmer Station seawater intake temperature at 6 m between January 2015 and May 2016. White region indicates the time period shown in panel b. Green line indicates height of warming period on January 20th. b) Bottom temperature recorded at mooring (dark gray line) and 40 m temperature (light gray line with diamonds) measured during biweekly water column sampling at Station E. Purple lines show temperature trends before January 20th (green dashed line) and orange lines show temperature trends after January 20th. c) Rates of warming before and after January 20th for all depths measured during biweekly sampling (profiles) and at seafloor (dots). Gray diamonds show slope data at 40 m, also shown in panel b.

Upper water column properties measured during biweekly sampling are shown on a temperature-salinity (TS) plot along with the bottom water properties measured by the mooring (Figure 4-4). Viewing the data in TS space reveals the unique water masses represented at this site. Surface waters are relatively fresh and warm during the summer, but cool to freezing and become saltier over winter as sea ice forms. This water mass, called Winter Water, can extend to 200 m and linger at depth during the following summer even as the surface warms and freshens from increased solar radiation, sea ice melt, and glacial runoff. The mooring deployment began in late November, three days after the last observation of Winter Water at the mooring site. Cross-canyon glider surveys during January 2015 revealed that the northern side of Palmer Deep retains more of its Winter Water than does the southern side of the canyon, where it is largely unobserved within the upper 100 m in summer [Carvalho *et al.*, 2016]. The mooring site is at the head of the canyon on the south side. TS characteristics from bottom measurements indicated modified UCDW throughout the deployment, oscillating between slightly cooler and fresher during one half of the tidal cycle and slightly warmer and saltier during the other half.

4.4.2 Currents and heat flux

Low-pass filtered current direction and speed are shown in Figure 4-5 along with daily wind vectors and sea ice concentration. Sea ice concentration at the mooring site exceeded 50% for most of early December and values of fluorescence, providing a measure of phytoplankton biomass, did not begin to rise above 1 mg m^{-3}

until mid-December (not shown). Observations are scarce in the upper half of the water column until mid-December, likely because there were few scatterers in the upper ocean until then.

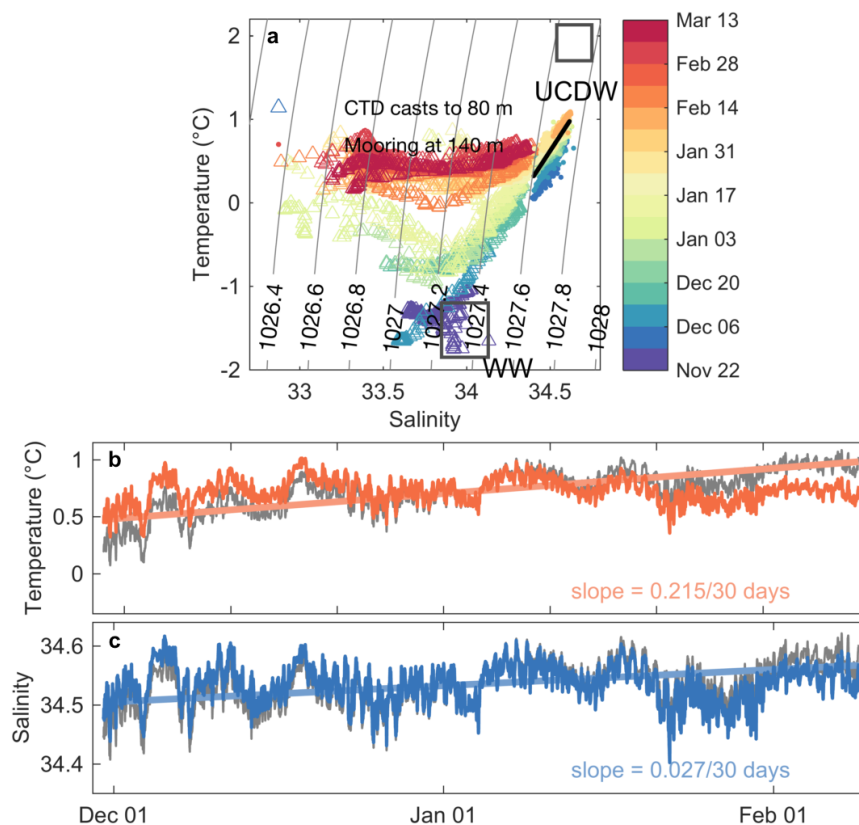


Figure 4-4: Temperature and salinity trends at the mooring site. a) Water column (triangles) and bottom (dots) temperature and salinity data plotted in TS space, colored by time of year. b) Original (gray) and detrended (orange) bottom temperature. c) Original (gray) and detrended (blue) bottom salinity. Trend lines that were removed from original data, and the slopes of those lines, are also shown in b and c.

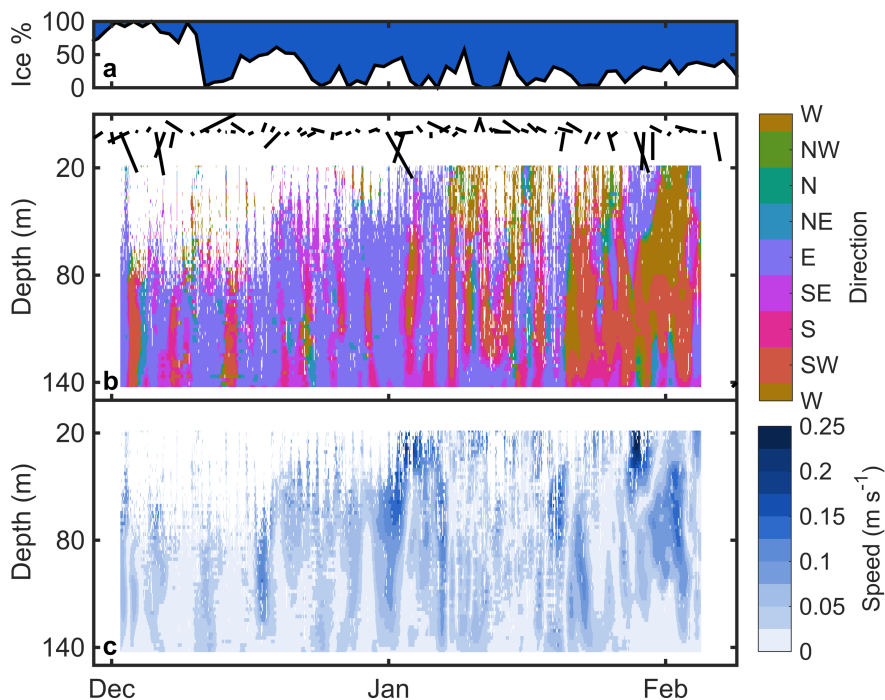


Figure 4-5: Sea ice concentration, and low-pass filtered wind direction, current direction, and current speed at Station E mooring site.

Currents throughout the water column were predominantly to the east and southeast until mid- to late January when the dominant direction became southwest. Bottom velocities rotated more slowly from almost due east to southeast over the duration of the deployment. The shift in bottom current direction was not as significant as the shift at shallower depths in the water column. Current speeds in the upper 100 m, and particularly in the upper 50 m, reached their highest values shortly after each of three strong northerly wind events beginning in early January. Current speeds in the upper 50 m were not well resolved until January so it is unclear whether similarly strong wind events led to a similar response before then.

Total, low-frequency and high-frequency components of heat and flux near the seafloor were calculated as follows:

$$\begin{aligned}
Q &= \rho c_p (T - T_f)(u + iv), \\
Q_{lp} &= \rho c_p (T_{lp} - T_f)(u_{lp} + iv_{lp}), \\
Q_{hp} &= \rho c_p (T_{hp} - T_f)(u_{hp} + iv_{hp}),
\end{aligned} \tag{4-1}$$

where c_p is the specific heat of seawater, ρ is the seawater density. T is the bottom temperature which is referenced to the freezing temperature of seawater, T_f . Eastward and northward components of bottom velocity are represented as u and v , respectively, and heat flux (Q) is separated into its low-pass (lp) and high-pass (hp) filtered components. Components of heat and flux were integrated over time to yield cumulative fluxes at the location of the mooring throughout its deployment duration.

Instantaneous bottom velocities oscillated from southwest to northeast throughout the deployment (Figure 4-6), defining the principle axis of motion. This axis aligns with the local bathymetry, closely following the 400 m isobath that extends from the head of Palmer Deep into Bismarck Strait (Figure 4-2). These high-frequency southwest-northeast oscillations were superimposed over a mean current that was directed to the east at the beginning of the deployment and rotated to the southeast by the end of the deployment (Figure 4-2).

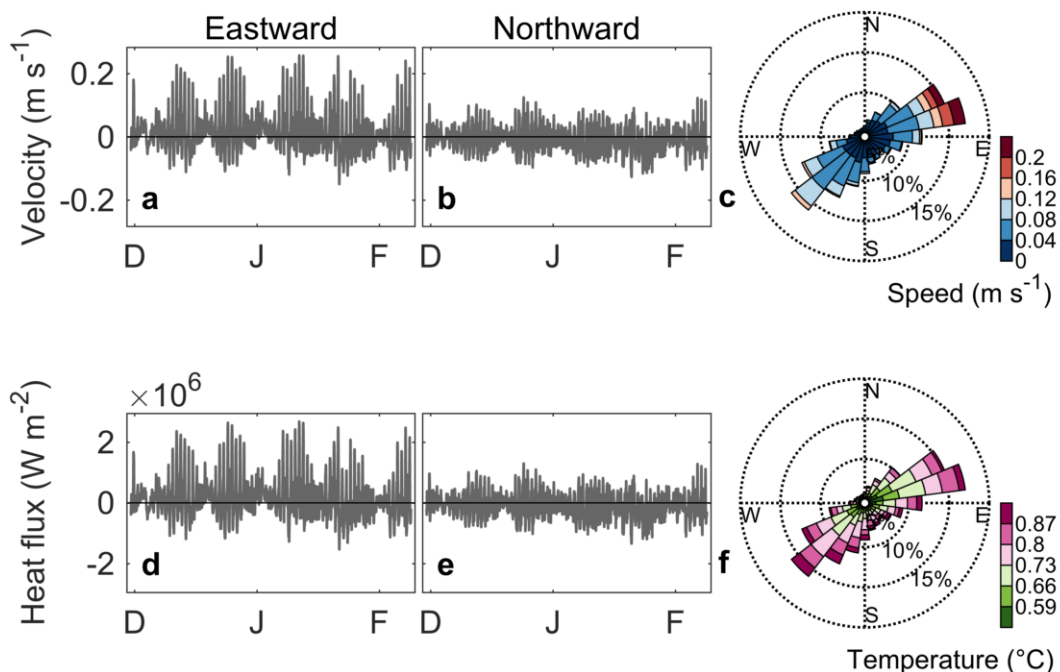


Figure 4-6: Time series and polar histograms of velocity and heat flux. a-b) Eastward and northward components of bottom velocity. c) Polar histogram of current direction colored by current speed. d-e) Eastward and northward components of bottom heat flux. f) Polar histogram of current direction colored by water temperature.

The high-pass filtered time series of velocity, temperature, and salinity reveal tidal patterns at the mooring site. The fastest speeds recorded throughout the deployment occur when current is flowing to the east/northeast, but currents flowing toward the southwest are slightly more common (Figure 4-8). This pattern describes a tidal cycle with a faster northeastward flood and a slower southwestward ebb. Warmer temperatures and higher salinities are associated with southwestward flow and cooler, fresher conditions are associated with northeastward flow. The low-frequency time series represent the sub-tidal time-averaged characteristics of the flow. Mean currents throughout the deployment were directed primarily to the east and southeast (Figure 4-7). The bottom

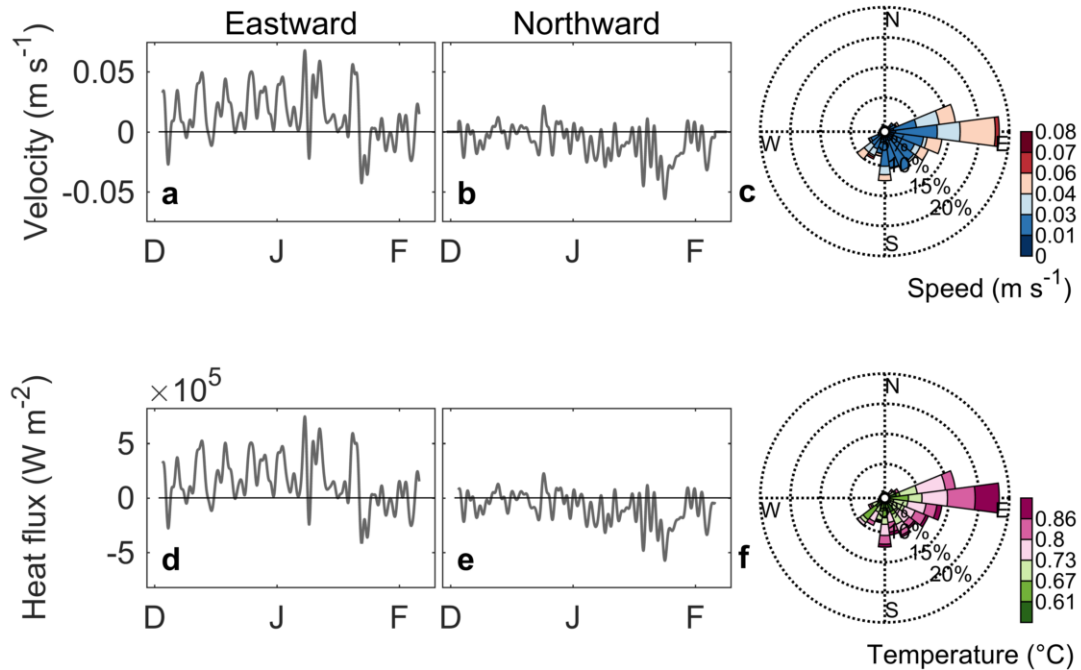


Figure 4-7: Time series and polar histograms of low-pass filtered velocity and heat flux.

a-b) Eastward and northward components of low-pass filtered bottom velocity. c) Polar histogram of low-pass filtered current direction colored by current speed. d-e) Eastward and northward components of low-pass filtered bottom heat flux. f) Polar histogram of low-pass filtered current direction colored by water temperature.

temperature increased from November to February such that the direction of the heat flux mirrored that of the current velocity.

The cumulative effect of these motions is shown in Figure 4-9. The low-frequency component of the bottom currents are almost exclusively responsible for the total heat flux toward the southeast, but they are modified slightly by tidally driven fluxes to the southwest.

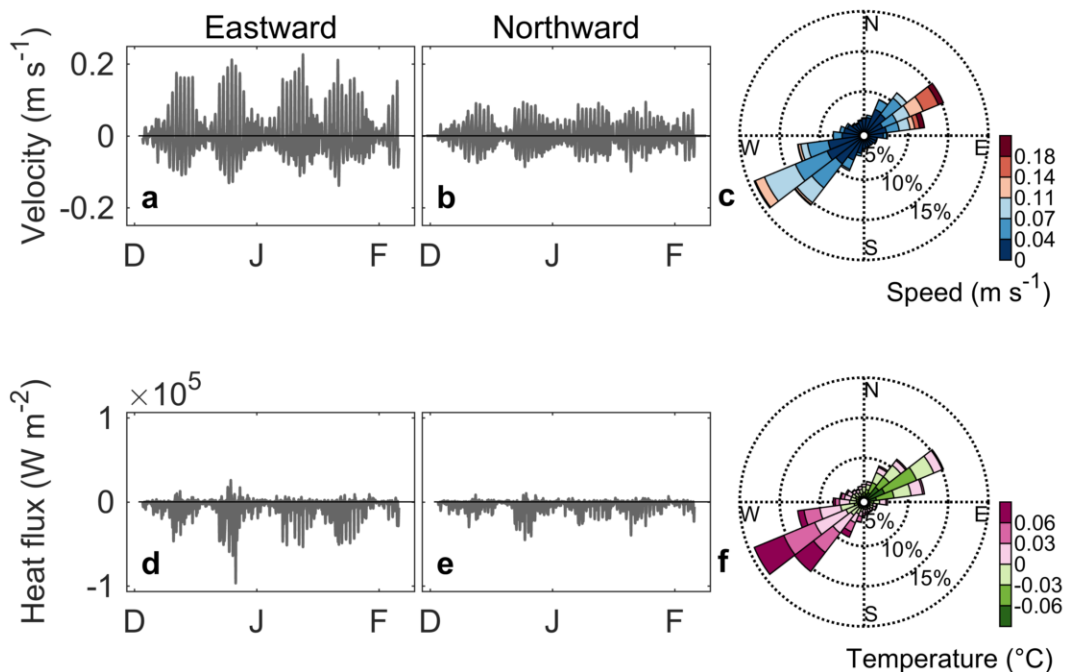


Figure 4-8: Time series and polar histograms of high-pass filtered velocity and heat flux.

a-b) Eastward and northward components of high-pass filtered bottom velocity. c) Polar histogram of high-pass filtered current direction colored by current speed. d-e) Eastward and northward components of high-pass filtered bottom heat flux. f) Polar histogram of high-pass filtered current direction colored by water temperature.

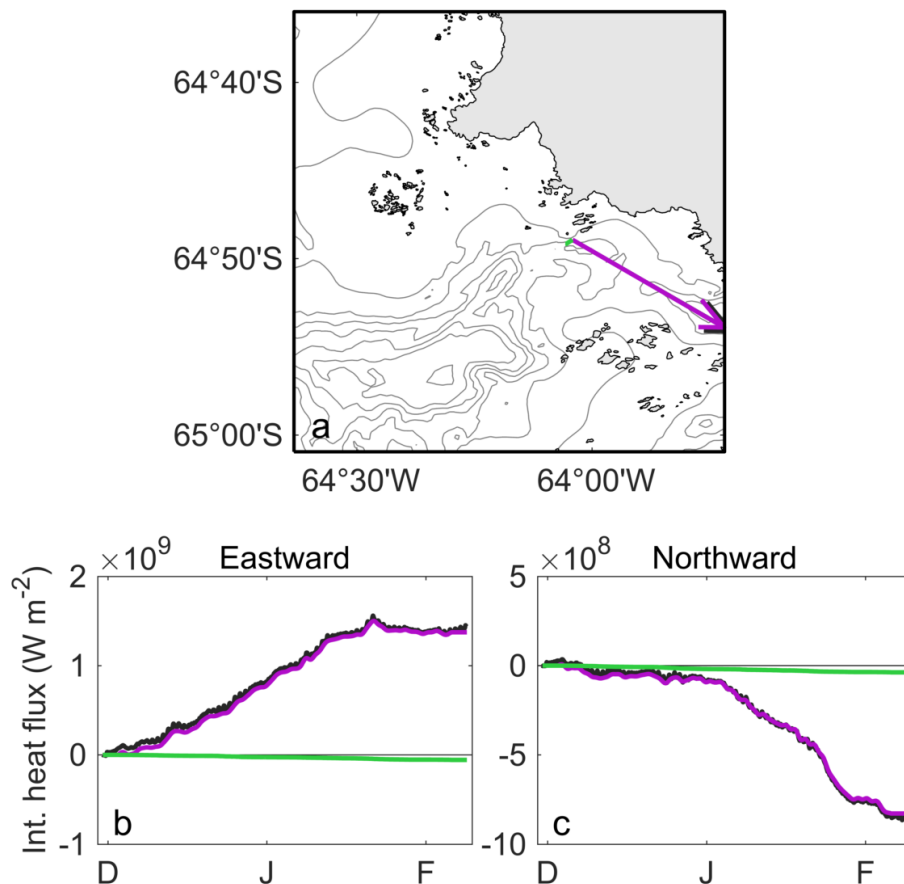


Figure 4-9: Integrated bottom heat flux over duration of mooring deployment. Relative contribution of high-frequency (green) and low-frequency (purple) components of total integrated heat flux (black) plotted as a) vectors emanated from mooring site (lengths vectors conserve the relative magnitude of the components, but their lengths compared to the map scale are meaningless), b) eastward components, and c) northward components.

4.4.3 Power spectral density estimates

Frequency analysis is a useful tool to expose the periodicity with which parameters vary and the relationships between them. We employ it here to investigate the relationships between wind forcing, current velocities throughout the water column, and bottom temperature. Power spectral density estimates of

wind, velocity and bottom temperature were calculated using the Welch method with a Hamming window the length of 2048 time points (corresponding to 14.2 days at a 10-minute sampling interval) with 50% overlap. This resulted in a spectral resolution of 0.07 cycles per day. Velocity and wind were rotated into “along-axis” and “across-axis” components, defined by the principle axis of motion of the depth-averaged currents measured at the mooring site throughout the deployment. This axis aligned with the curvature of the local bathymetry (Figure 4-2), and depth-averaged velocities oscillated back and forth along it at tidal frequencies.

Power spectral densities of four parameters were estimated in the along- and across-axis direction: Palmer Station wind velocity, bottom water temperature at Station E, mid-water column velocity, and near-bottom current velocity. Power estimates were highest for the three water column variables at diurnal and semidiurnal frequencies and all four variables showed a trend of increasing power at low frequencies, consistent with red noise. A common trend among atmospheric and hydrographic data with high level of autocorrelation between successive measurements is that relative variance decreases at higher frequencies and increases at lower frequencies leading to a background spectrum of “red noise” [Gilman and Fuglister, 1963]. The higher the degree of autocorrelation in a time series, the more “memory” that parameter has of its previous state and the higher the power will be at low frequencies. The red noise spectrum, which is equivalent to the spectrum a first-order autoregressive process with positive correlation at one lag [von Storch and Zwiers, 1999], represents the null hypothesis of significance. The

significance of a power spectral density estimate can be assessed by comparing it to the red noise spectrum, which is calculated following Gilman 1963 as:

$$P = \frac{1 - \rho^2}{1 - 2\rho \cos\left(\frac{h\pi}{M}\right) + \rho^2}, \quad (4-2)$$

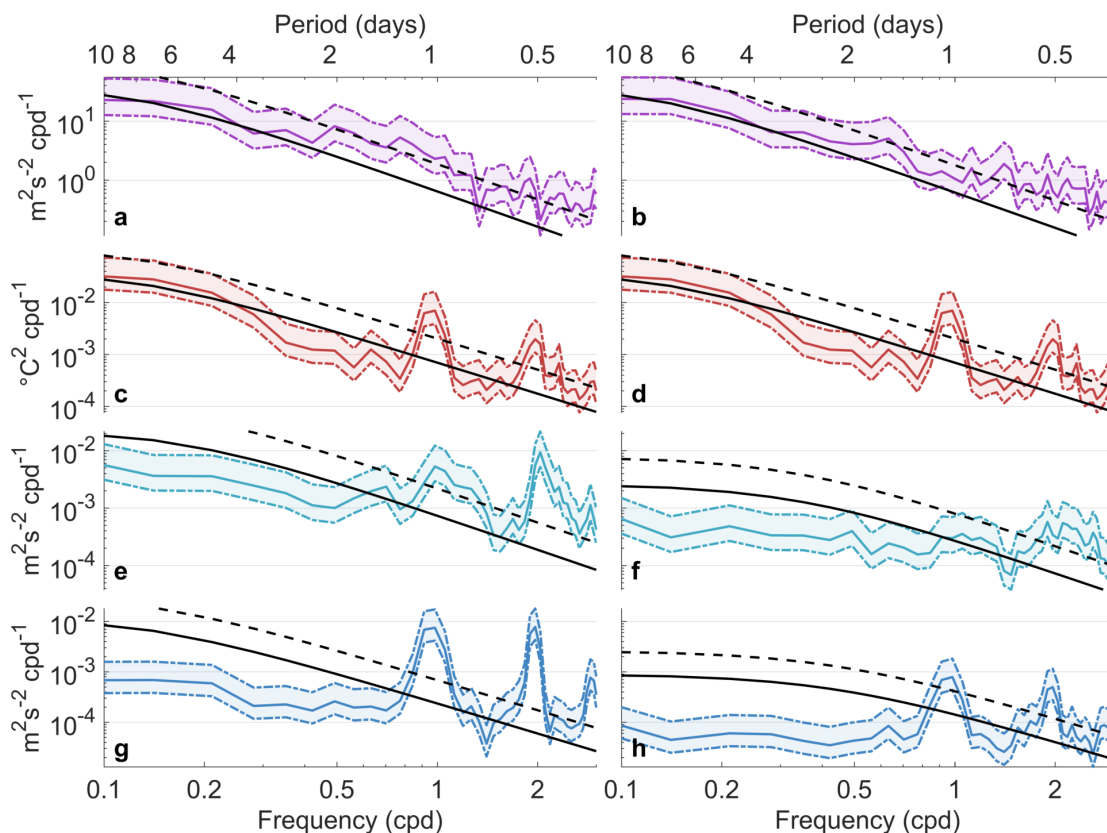


Figure 4-10: Power spectral densities of wind, bottom temperature, and current velocities.

Power spectral density of a-b) wind velocity at Palmer Station, and c-d) bottom temperature, e-f) 83 m current velocity, and g-h) 143 m current velocity at Station E in the along-axis direction (left column) and across-axis direction (right column). (The power spectral density of temperature is not separated into along- and across-axis components. The same plot is duplicated in panels c and d). Colored shading shows the 95% confidence interval of spectral estimates. Solid black lines show the red noise spectra and dashed black lines show the 95% confidence level of red noise spectra.

where ρ is the one-lag autocorrelation and M is half the length of the Hamming window used to calculate the power spectral densities. M also represents the maximum number of lags and h represents the resolved frequencies in integers varying from zero to M .

With the exception of power near diurnal and semi-diurnal frequencies, which is strong for the three sets of water column observations, the power spectral densities of wind, current velocities, and bottom temperature are mostly indistinguishable from red noise at the 95% confidence level (Figure 4-10). There is more power in the along-axis component of velocity than the across-axis, which is expected since the along-axis direction was chosen based on the principal components of velocity. There is approximately equal power in the along- and across-axis components of wind.

4.4.4 Coherence

Although the power spectra of wind, velocity, and temperature are mostly indistinguishable from red noise outside the diurnal and semidiurnal frequency bands, there may still be some coherency between variables at other frequencies. Coherence measures the association between two parameters at a given frequency. Values range from 0 to 1 with higher values indicating a stronger relationship at that frequency, perhaps with a phase difference by which one signal lags the other. We calculate estimates of magnitude-squared coherence and the associated phase shift between the wind, bottom velocity and temperature to test for coherent modes

among data sets (Figure 4-11 through Figure 4-13). Coherence-squared is evaluated at the 95% confidence level following Thompson [1979]:

$$\gamma^2 = 1 - \alpha^{[1/(EDOF-1)]}, \quad (4-3)$$

where $\alpha = 1 - 0.95$ and $EDOF$ is the equivalent degrees of freedom. $EDOF$ for spectra calculated using a Hamming window, as we have done here, is $2.5164(N/M)$ where N is the number of data points and M is half the window length. For this dataset, values above 0.117 are considered significant. Phase lags in degrees are converted to lags in days by noting that, for a given frequency, a phase of 2π indicates that one signal lags the other by the time required to complete a full period:

$$time\ lag\ (days) = \frac{phase\ (rad)}{2\pi f}, \quad (4-4)$$

where f is the frequency.

Coherence is measured between wind velocity at Palmer Station and bottom velocity at the Station E mooring (Figure 4-11). The along-axis component of the wind is more strongly coherent than the across-axis component with along-axis bottom velocity, suggested a direct influence of wind forcing on the current direction, rather than a wind-driven Ekman transport. The highest values of coherence for both components of wind velocity occur for periods between 5 and 8 days. This period range corresponds to the 0.15-0.25 cpd frequency band where the subtidal power spectral density of the wind was also highest (Figure 4-10). Along-axis bottom velocity had a higher power spectral density in this frequency band than the across-axis component as well. In this frequency band, current velocity lagged the wind by 2-4 days. This response time can also be seen in Figure 4-5: after

the strongest wind events, a significant change in the direction of the low-frequency current followed 2-4 days later. The across-axis component of bottom velocity is weakly coherent with both components of the wind, and only in the 2-3 day range.

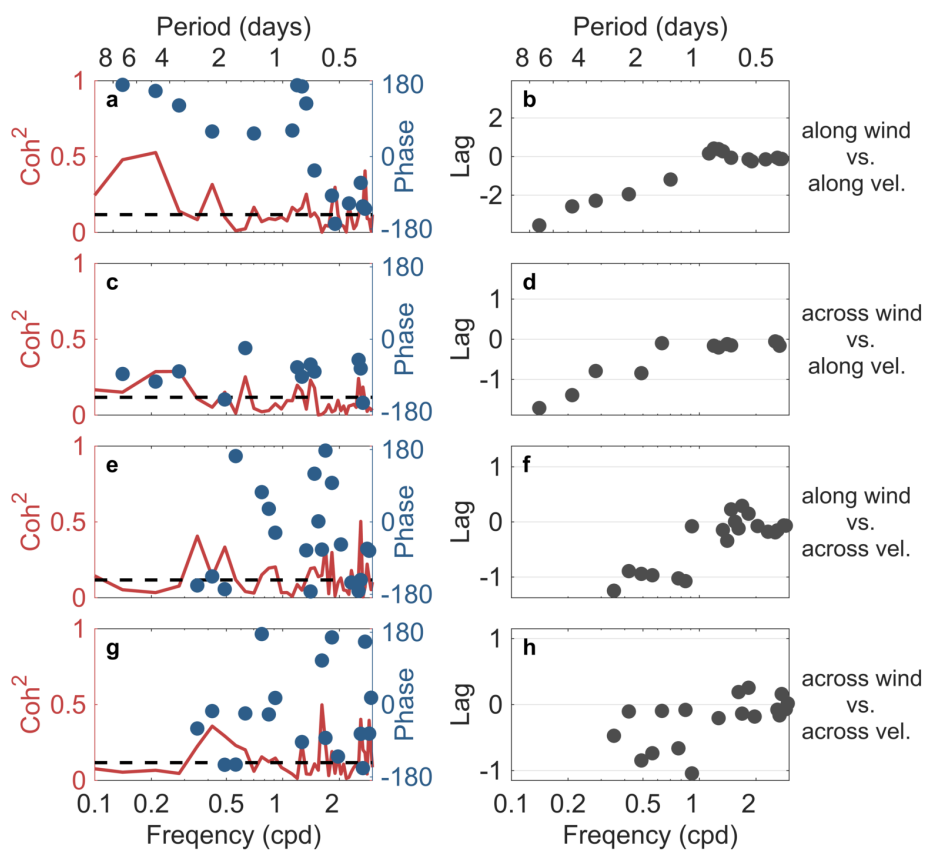


Figure 4-11: Coherence and phase lag between wind and bottom velocity. Magnitude-squared coherence and phase lag in degrees are shown between a) along-axis component of Palmer Station wind and along-axis component of Station E bottom velocity, c) across-axis wind and along-axis velocity, e) along-axis wind and across-axis velocity, and g) across-axis wind and across-axis velocity. Phase lags in degrees are converted to days and shown in panels b,d,f, and h.

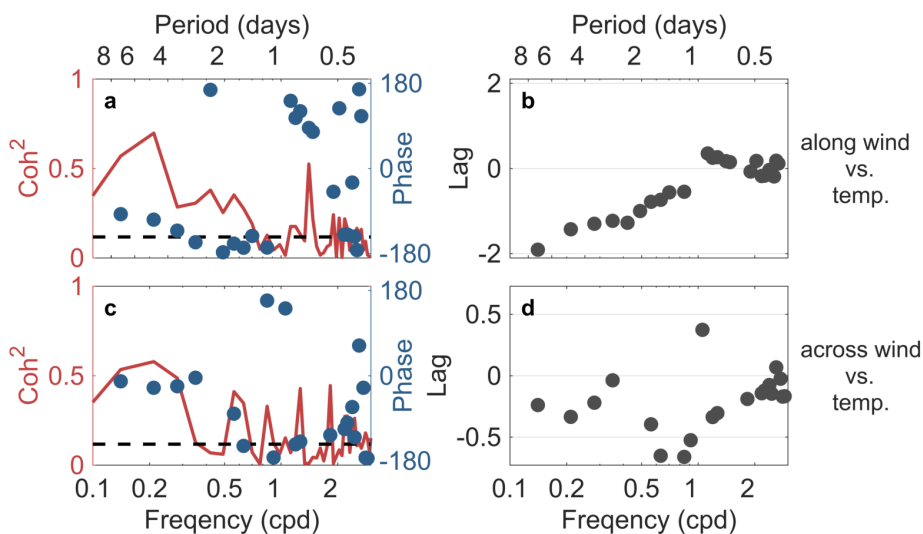


Figure 4-12: Coherence and phase lag between wind and bottom temperature. Magnitude-squared coherence and phase lag in degrees are shown between a) along-axis component of Palmer Station wind and Station E bottom temperature, c) across-axis wind and bottom temperature. Phase lags in degrees are converted to days and shown in panels b and d.

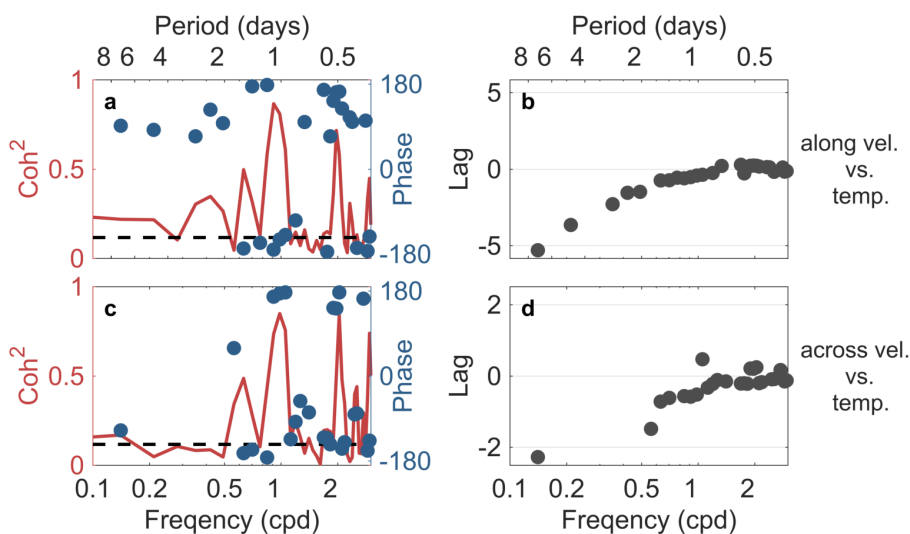


Figure 4-13: Coherence and phase lag between bottom velocity and bottom temperature. Magnitude-squared coherence and phase lag in degrees are shown between a) along-axis component of Station E bottom velocity and bottom temperature, c) across-axis velocity and bottom temperature. Phase lags in degrees are converted to days and shown in panels b and d.

Along-axis wind and bottom temperature are significantly coherent over a wider range of frequencies than are across-axis wind and temperature. The along-axis wind is associated with a 1-2 day delay in temperature at periods greater than 2 days while the across-axis component of wind is associated with a less significant but more immediate temperature response. Bottom velocity and temperature are strongly coherent and 180° out of phase for high frequencies coinciding with the diurnal and semidiurnal tidal bands. This is consistent with the heat flux analysis: when along-axis velocity is most positive (maximum flood), temperature is coolest, and when along-axis velocity is most negative (maximum ebb), temperature is warmest. There is weak but significant coherence between velocity and temperature at sub-tidal frequencies.

4.5 Discussion

4.5.1 Influence of the Antarctic Peninsula Coastal Current and winds on local circulation

Low-pass filtered current velocities revealed flow to the east throughout the water column from late November through early January (Figure 4-5). From early January until the end of the deployment in early February, flow was increasingly toward the southwest, particularly after northerly wind events. These observations are consistent with the description by Savidge and Amft [2009] of a current moving counter-clockwise around Anvers Island that is stronger during winter than summer. Between depths of 40 and 200 m, the southward flow along the west coast of Anvers Island was described as being part of the APCC, and a northeastward-

flowing branch into Gerlache Strait was hypothesized to either be a continuation of the APCC or the result of topographically controlled circulation around the island [Savidge and Amft, 2009]. Station E is located between these two branches such that a current flowing past the mooring that connects the two branches should travel toward the southeast or east. Eastward flow was common in the early part of the mooring deployment, but flow shifted toward the southwest later in the season, consistent with this northern branch of the APCC weakening in the summer.

Further south on the WAP shelf, west of Adelaide Island and within Marguerite Bay, the APCC is stronger during summer when increased glacial melt water and sea ice melt help to sustain the geostrophically-balanced buoyancy-forced current [Moffat *et al.*, 2008; Savidge and Amft, 2009]. A possible explanation for the difference in seasonality between the APCC near Anvers and the APCC near Adelaide Island is the different effect that northerly winds have on the sea ice environment in each area. Northerly winds tend to push sea ice away from the northern part of the WAP toward the south where ice accumulates and melts [Stammerjohn *et al.*, 2008b; Meredith *et al.*, 2017]. Surface layer salinity decreases from north to south [Meredith *et al.*, 2017] with the highest freshwater content in the WAP surface waters found in Marguerite Bay [Stammerjohn *et al.*, 2008a]. The opening of the surface ocean in the north exposes it to wind forcing, leading to a more wind-driven flow and weakening the net effect of the APCC in the north. In the south, the increased volume of freshwater at the surface strengthens the buoyant plume that supports the APCC. Southward currents at Station E at the end of the deployment are consistent with northerly wind forcing.

Sea ice coverage at the mooring site was almost 100% until early to mid-December (Figure 4-5). Winds during the ice-covered period were often strong and northerly, but they were significantly weaker in the latter half of December. Throughout this early period, currents throughout the water column were largely barotropic and primarily directed to the east and southeast. A strong northerly wind event occurred at the beginning of January, which was quickly followed by southwestward flow throughout the water column. Throughout the latter half of January, winds were consistently from the north and low-pass filtered velocities were increasingly to the southwest. Throughout this period, sea ice concentration was relatively low.

Winds are known to be highly variable on the WAP, with monthly variance in wind velocity often exceeding the mean [*Beardsley et al., 2004*]. Bottom velocities at Station E were most strongly coherent with wind speeds in the 0.15-0.25 cpd frequency band, corresponding to a period of 5-8 days. The synoptic time scale on the WAP, that is, the period at which weather systems tend to pass through, is 2-8 days [*Dinniman et al., 2011*]. Bottom velocities lagged the wind by 2-4 days. A similar lag has been identified between wind forcing along the continental shelf and volume transport at the shelf break near Marguerite Trough.

The along-axis component of bottom velocity, which closely aligns with the direction of tidal fluctuations but generally not with the mean current, is coherent with along-axis wind at periods of 4-8 days. However, the across-axis component of bottom velocity, which generally aligns with the direction of mean flow, is not strongly coherent with either component of the wind. This is consistent with a mean

current that is driven on a more regional and long-term scale by the APCC and less by the local variable winds. Along-axis winds did begin to align with the mean current near the end of the deployment, which could be affecting the stronger coherence between along-axis wind and along-axis velocity.

4.5.2 Local tidal fluctuations

The high-pass filtered time series of velocity, temperature, and salinity at the seafloor of the mooring site lend insight about the physical environment immediately surrounding Station E. Warmer temperatures were associated with the ebb (southeastward) and cooler temperatures were associated with the flood (northeastward, Figure 4-8). This pattern describes an environment in which water temperatures are warmer on the northeast side of the mooring than on the southwest side. This is a somewhat counterintuitive result since it is thought that the canyons in this region provide a conduit for warm mUCDW to flow through, and the mooring sits at the head of one such canyon. Upwelling of warm sub-pycnocline water has been observed on the southern side of Palmer Deep [*Carvalho et al.*, 2016; *Schofield et al.*, 2017b] with warmer deep waters intruding into the upper 100 m. Noting the location of the mooring observations on the seafloor at the edge of a sharp slope into Bismarck Strait, the direction of the tidal heat flux is, indeed, consistent with upwelling observations in this area and suggests that the upward sloping of isopycnals at the canyon head is a consistent feature during spring and summer. The mooring sat at 143 m on the ledge of a trough. Sloping isopycnals at the trough wall would lead to warmer temperatures at 143 m on the ledge than at

143 m out in the center of the trough. This slope-derived gradient in temperature would lead to warm water moving out toward the center of the trough on the ebb and cooler water moving toward the ledge on the flood.

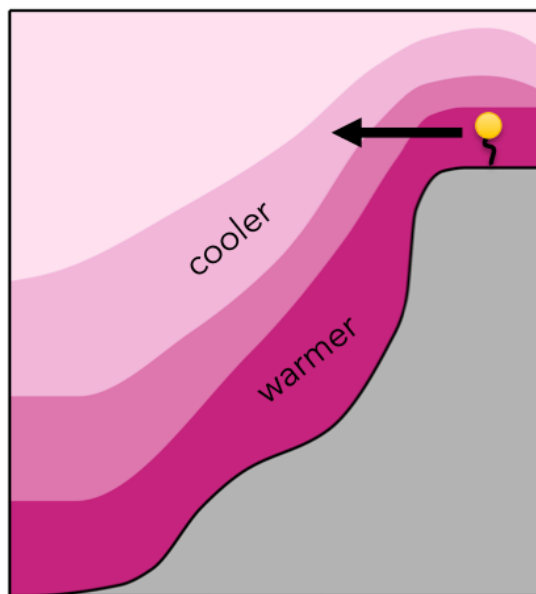


Figure 4-14 Schematic of upwelling at the mooring location. Arrow indicates direction of high-pass filtered heat flux.

4.6 Conclusions

Circulation at Station E is dependent on ice cover, wind forcing, and the strength of the APCC. Observations from a mooring deployed at Station E from late spring to mid-summer in 2015 and 2016 represent conditions from the end of the ice-covered season and into the ice-free season. During winter, the strongest driver of current velocity appears to be the APCC and its topographically-steered counter-clockwise flow around Anvers Island, moving water toward the southeast. As the ice melted during summer, exposing the upper ocean to the winds, the ocean became

more responsive to the wind. As winds became increasingly northerly, the depth-averaged flow was directed more to the southwest.

Wind stresses along the WAP have increased in recent decades [*Stammerjohn et al., 2008a*] leading to a decrease in sea ice thickness and the length of the sea ice season [*Stammerjohn et al., 2008b; Montes-Hugo et al., 2009*]. Since 2009, however, there has been an increase in sea ice at Palmer Station. Increased study of the APCC in the northern WAP is necessary to determine what the effects of an increasingly ice-free ocean may be. This branch of the APCC appears to begin south of Bransfield Strait [*Moffat et al., 2008; Savidge and Amft, 2009*] and is likely to be influenced both by cold Weddell-sourced waters and by UCDW from the WAP shelf break, but the relative importance of each of these is unknown. The results presented here suggest that strengthening northerly winds would lead to a weaker APCC in the northern WAP. The net heat flux in the LTER sampling area near Palmer Station is dominated by the southeastward flow, so changes in its strength are likely to be important in controlling physical environment that supports biological communities in the area.

5 Summary and Conclusions

The West Antarctic Peninsula continental shelf is an ecologically important area in the Southern Ocean, supporting biological hotspots that sustain extensive krill populations and many of the higher trophic levels in the Antarctic food web. The region is also undergoing rapid climatic change that is certain to have a significant impact on the physical and ecological landscapes. Increases in ocean and air temperatures have contributed to a decrease in glacial ice mass and a shortening of the annual sea ice season. Ocean processes play an important role in the redistribution of heat that is driving these changes, but these processes are still poorly understood. Observations around Antarctica remain scarce compared to other regions of the world ocean due to the logistical challenges of sampling, particularly during winter. However, technological advances in recent decades have vastly improved our ability to collect measurements and the combination of continued observations and regional numeric modeling continue to advance our understanding of this important system.

This dissertation uses observations from one of the longest-running time series of hydrographic data in Antarctica, collected by the Palmer Station Long Term Ecological Research project. More recent datasets from glider deployments, moored instruments, and model output complement these historic shelf-wide observations and allow us to investigate processes affecting heat transport that occur at different temporal and spatial scales.

Gliders were used in Chapter 2 to map the distribution of UCDW on the WAP shelf and to identify subsurface eddies containing modified UCDW. Previous studies identified eddies following the northeast wall of Marguerite Trough across the shelf and suggested that eddies were the dominant mechanism bringing UCDW to the WAP shelf [Moffat *et al.*, 2009; Martinson, 2012]. Marguerite Trough was found to be an important conduit for eddies moving across the shelf, but eddies were also observed in other cross-shelf troughs to the north. We concluded that eddies contribute up to 50% of the heat entering the shelf and that they lose heat at a steady rate as they follow bathymetric features on the shelf.

Chapter 3 focused on the circulation pathways that carry UCDW from the shelf break to Palmer Deep, an ecologically important canyon in the northern part of the WAP. Virtual drifters released in the subsurface waters containing UCDW along the shelf slope were found to travel northward along the slope until they were pulled into the shelf interior at one of the cross-shelf troughs that open at the shelf break. Circulation in these troughs was cyclonic, such that drifters were pulled in on the northern sides and often continued looping clockwise, flowing back toward the shelf break on the southern side. Water that began as UCDW was modified by the time it reached Palmer Deep. It was found that particles that drifted far enough to the north that they encountered Bransfield Strait waters had cooled the most upon entry to Palmer Deep.

In Chapter 4, we investigated the factors influencing current velocity and heat flux at the head of Palmer Deep canyon. Observations were made at high temporal resolution during a 10-week period at the end of spring and the beginning

of summer. We found a significant change in the mean depth-averaged current direction between the beginning of observations when sea ice was still present and the end of observations, when sea ice had disappeared and winds from the north had intensified. The change was attributed to the weakening of the Antarctic Peninsula Coastal Current during summer and the increased effect of winds on the water column during the ice-free season.

This dissertation provides estimates of rates of heat transport across the WAP and to the ecologically important Palmer Deep canyon. It concludes that the shelf-crossing troughs are important for moving heat to the shelf interior and nearshore regions, but that circulation pathways are complicated and seasonally variable. Climatic changes are expected to continue over the WAP. Winds over the northern part of the peninsula have strengthened in recent decades leading to shorter sea ice seasons [*Stammerjohn et al., 2008b; Montes-Hugo et al., 2009*] and increased heat flux across the shelf break [*Martinson et al., 2008*]. Transport via cross-shelf troughs will be affected by changes in the wind and, while the northern trough remains under-sampled, eddies were observed along its northeast wall and are likely important to heat transport in that region. Northerly winds were shown to decrease the rate of heat flux associated with the Antarctic Peninsula Coastal Current along Anvers Island. A continued observation effort focused on circulation in the northern trough system will improve our understanding of the Palmer Deep ecosystem and how coastal canyon systems like it are likely to react to changing conditions.

Acknowledgement of Previous Publications

Chapter 1 has been published in the scientific research journal *Journal of Geophysical Research: Oceans*:

Couto, N., D. G. Martinson, J. Kohut, and O. Schofield (2017), Distribution of upper circumpolar Deep Water on the warming continental shelf of the West Antarctic Peninsula, *Journal of Geophysical Research: Oceans*, doi:10.1002/2017JC012840.

References

- Allen, S. E., C. Vindeirinho, R. E. Thomson, M. G. G. Foreman, and D. L. Mackas (2001), Physical and biological processes over a submarine canyon during an upwelling event, *Can. J. Fish. Aquat. Sci.*, 58(4), 671–684, doi:10.1139/cjfas-58-4-671.
- Ashjian, C. J., C. S. Davis, S. M. Gallagher, P. H. Wiebe, and G. L. Lawson (2008), Distribution of larval krill and zooplankton in association with hydrography in Marguerite Bay, Antarctic Peninsula, in austral fall and winter 2001 described using the Video Plankton Recorder, *Deep Sea Research Part II: Topical Studies in Oceanography*, 55(3-4), 455–471, doi:10.1016/j.dsr2.2007.11.016.
- Beardsley, R. C., R. Limeburner, and W. Brechner Owens (2004), Drifter measurements of surface currents near Marguerite Bay on the western Antarctic Peninsula shelf during austral summer and fall, 2001 and 2002, *Deep Sea Research II*, 51(17-19), 1947–1964, doi:10.1016/j.dsr2.2004.07.031.
- Beitsch, A., L. Kaleschke, and S. Kern (2013), *AMSR2 ASI 3.125 km Sea ice concentration data, V0. 1, Institute of Oceanography, University of Hamburg, Germany, digital media.*
- Bernard, K. S., and D. K. Steinberg (2013), Krill biomass and aggregation structure in relation to tidal cycle in a penguin foraging region off the Western Antarctic Peninsula, *ICES J. Mar. Sci.*, 70(4), 834–849, doi:10.1093/icesjms/fst088.
- Bernard, K. S., M. Cimino, W. Fraser, J. Kohut, M. J. Oliver, D. Patterson-Fraser, O. M. E. Schofield, H. Statscewich, D. K. Steinberg, and P. Winsor (2017), Factors that affect the nearshore aggregations of Antarctic krill in a biological hotspot, *Deep-Sea Research Part I*, doi:10.1016/j.dsr.2017.05.008.
- Bower, A. S., R. M. Hendry, D. E. Amrhein, and J. M. Lilly (2013), Direct observations of formation and propagation of subpolar eddies into the Subtropical North Atlantic, *Deep Sea Research Part II: Topical Studies in Oceanography*, 85, 15–41, doi:10.1016/j.dsr2.2012.07.029.
- Bromwich, D. H., J. P. Nicolas, A. J. Monaghan, M. A. Lazzara, L. M. Keller, G. A. Weidner, and A. B. Wilson (2013), Central West Antarctica among the most rapidly warming regions on Earth, *Nature Geoscience*, 6, 139–145.
- Budgell, W. P. (2005), Numerical simulation of ice-ocean variability in the Barents Sea region, *Ocean Dynamics*, 55(3-4), 370–387, doi:10.1007/s10236-005-0008-3.
- Carvalho, F., J. Kohut, M. J. Oliver, R. M. Sherrell, and O. Schofield (2016), Mixing and

- phytoplankton dynamics in a submarine canyon in the West Antarctic Peninsula, *Journal of Geophysical Research: Oceans*, 121(7), 5069–5083, doi:10.1002/2016JC011650.
- Chelton, D. B., R. A. deSzoeko, M. G. Schlax, K. El Naggar, N. Siwertz, D. B. Chelton, R. A. deSzoeko, M. G. Schlax, K. El Naggar, and N. Siwertz (1998), Geographical Variability of the First Baroclinic Rossby Radius of Deformation, [http://dx.doi.org/10.1175/1520-0485\(1998\)028<0433:GVOTFB>2.0.CO;2](http://dx.doi.org/10.1175/1520-0485(1998)028<0433:GVOTFB>2.0.CO;2), 28(3), 433–460, doi:10.1175/1520-0485(1998)028<0433:GVOTFB>2.0.CO;2.
- Cook, A. J., A. J. Fox, D. G. Vaughan, and J. G. Ferrigno (2005), Retreating Glacier Fronts on the Antarctic Peninsula over the Past Half-Century, *Science*, 308(5721), 541–544, doi:10.1126/science.1104235.
- Cook, A. J., P. R. Holland, M. P. Meredith, T. Murray, A. Luckman, and D. G. Vaughan (2016), Ocean forcing of glacier retreat in the western Antarctic Peninsula, *Science*, 353(6296), 283–286, doi:10.1126/science.aae0017.
- Couto, N., D. G. Martinson, J. Kohut, and O. Schofield (2017), Distribution of upper circumpolar Deep Water on the warming continental shelf of the West Antarctic Peninsula, *Journal of Geophysical Research: Oceans*, doi:10.1002/2017JC012840.
- Davis, R. E., C. C. Eriksen, and C. P. Jones (2002), Autonomous buoyancy-driven underwater gliders, in *The technology and applications of autonomous underwater vehicles*, edited by G. Griffiths, pp. 37–58, Taylor and Francis, London.
- Dinniman, M. S., and J. M. Klinck (2004), A model study of circulation and cross-shelf exchange on the west Antarctic Peninsula continental shelf, *Deep Sea Research Part II: Topical Studies in Oceanography*, 51, 2003–2022.
- Dinniman, M. S., J. M. Klinck, and W. O. Smith (2007), Influence of sea ice cover and icebergs on circulation and water mass formation in a numerical circulation model of the Ross Sea, Antarctica, *Journal of Geophysical Research: Oceans*, 112(C11), 57, doi:10.1029/2006JC004036.
- Dinniman, M. S., Klinck, J. M., and W. O. Smith Jr. (2011), A model study of Circumpolar Deep Water on the West Antarctic Peninsula and Ross Sea continental shelves, *Deep Sea Research II*, 58(13-16), 1508–1523, doi:10.1016/j.dsr2.2010.11.013.
- Donnelly, J., and J. J. Torres (2008), Pelagic fishes in the Marguerite Bay region of the West Antarctic Peninsula continental shelf, *Deep Sea Research II*, 55(3-4), 523–539, doi:10.1016/j.dsr2.2007.11.015.
- Ducklow, H. et al. (2012), The Marine System of the Western Antarctic Peninsula, in *Antarctic Ecosystems An Extreme Environment in a Changing World*, edited by A.

D. Rogers, N. M. Johnston, E. J. Murphy, and A. Clarke, Blackwell Publishing Ltd., London.

- Ducklow, H. et al. (2013), West Antarctic Peninsula: An Ice-Dependent Coastal Marine Ecosystem in Transition, *Oceanography*, 26(3), 190–203, doi:10.5670/oceanog.2013.62.
- Ducklow, H., Martinson, D. G., K. S. Baker, L. B. Quetin, R. M. Ross, R. C. Smith, S. E. Stammerjohn, M. Vernet, and W. Fraser (2007), Marine pelagic ecosystems: the West Antarctic Peninsula, *Philosophical Transactions of the Royal Society B: Biological Sciences*, 362(1477), 67–94, doi:10.1098/rstb.2006.1955.
- Erickson, Z. K., A. F. Thompson, N. Cassar, J. Sprintall, and M. R. Mazloff (2016), An advective mechanism for deep chlorophyll maxima formation in southern Drake Passage, *Geophysical Research Letters*, 43(20), 10,846–10,855, doi:10.1002/2016GL070565.
- Fretwell, P. et al. (2013), Bedmap2: improved ice bed, surface and thickness datasets for Antarctica, *The Cryosphere*, 7(1), 375–393, doi:10.5194/tc-7-375-2013.
- Genin, A. (2004), Bio-physical coupling in the formation of zooplankton and fish aggregations over abrupt topographies, *Journal of Marine Systems*, 50(1-2), 3–20, doi:10.1016/j.jmarsys.2003.10.008.
- Gilman, D. L., and F. J. Fuglister (1963), On the power spectrum of “red noise,” *Journal of the ...*
- Graham, J. A., and M. S. Dinniman (2016), Impact of model resolution for on-shelf heat transport along the West Antarctic Peninsula, *Journal of Geophysical Research: Oceans*, doi:10.1002/2016JC011875.
- Graham, J. A., M. S. Dinniman, and J. M. Klinck (2016), Impact of model resolution for on-shelf heat transport along the West Antarctic Peninsula, *Journal of Geophysical Research: Oceans*, 121(10), 7880–7897, doi:10.1002/2016JC011875.
- H. Van Loon (1967), The Half-Yearly Oscillations in Middle and High Southern Latitudes and the Coreless Winter, *Journal of the Atmospheric Sciences*, 24(5), 472–486, doi:10.1175/1520-0469(1967)024<0472:THYOIM>2.0.CO;2.
- Henley, S. F., R. E. Tuerena, A. L. Annett, A. E. Fallick, M. P. Meredith, H. J. Venables, A. Clarke, and R. S. Ganeshram (2017), Macronutrient supply, uptake and recycling in the coastal ocean of the west Antarctic Peninsula, *Deep Sea Research Part II: Topical Studies in Oceanography*, 139, 58–76, doi:10.1016/j.dsr2.2016.10.003.
- Heywood, K. J. et al. (2014), Ocean processes at the Antarctic continental slope, *Phil. Trans. R. Soc. A*, 372(2019), 20130047–20130047, doi:10.1098/rsta.2013.0047.

- Heywood, K. J., A. C. Naveira Garabato, D. P. Stevens, and R. D. Muench (2004), On the fate of the Antarctic Slope Front and the origin of the Weddell Front, *Journal of Geophysical Research: Oceans*, 109(C6), 1173, doi:10.1029/2003JC002053.
- Hickey, B. M. (1995), Coastal submarine canyons, in *Proceedings of the University of Hawaii Aha Hulikoa Workshop on Flow Topography Interactions. SOEST Special Publication*, edited by P. Muller and D. Henderson, pp. 95–110, Topographic effects in the ocean.
- Hofmann, E. E., J. M. Klinck, C. M. Lascara, and D. A. Smith (1996), Water mass distribution and circulation west of the Antarctic Peninsula and including Bransfield Strait, in *Foundations for Ecological Research West of the Antarctic Peninsula*, vol. Washington, DC, edited by R. M. Ross, E. E. Hofmann, and L. B. Quentin, pp. 61–80, American Geophysical Union.
- Howard, S. L., J. Hyatt, and L. Padman (2004), Mixing in the pycnocline over the western Antarctic Peninsula shelf during Southern Ocean GLOBEC, *Deep Sea Research Part II: Topical Studies in Oceanography*, 51(17-19), 1965–1979, doi:10.1016/j.dsr2.2004.08.002.
- Huss, M., and D. Farinotti (2014), A high-resolution bedrock map for the Antarctic Peninsula, *The Cryosphere*.
- Jenkins, A., P. Dutrieux, S. S. Jacobs, S. D. McPhail, J. R. Perrett, A. T. Webb, and D. White (2010), Observations beneath Pine Island Glacier in West Antarctica and implications for its retreat, *Nature Geoscience*, 3(7), 468–472, doi:10.1038/ngeo890.
- Kavanaugh, M. T., F. N. Abdala, H. Ducklow, and D. M. Glover (2015), Effect of continental shelf canyons on phytoplankton biomass and community composition along the western Antarctic Peninsula, *Mar. Ecol. Prog. Ser.*, 524, 11–26, doi:10.3354/meps11189.
- Klinck, J. M. (1995), *Comparison between a global tide model and observed tides at Palmer Station*, Antarctic Journal of the United States.
- Klinck, J. M. (1998), Heat and salt changes on the continental shelf west of the Antarctic Peninsula between January 1993 and January 1994, *Journal of Geophysical Research: Oceans*, 103, 7617–7636, doi:10.1029/98JC00369.
- Klinck, J. M., and M. S. Dinniman (2010), Exchange across the shelf break at high southern latitudes, *Ocean Science Discussions*, 6, 513–524, doi:10.5194/os-6-513-2010.
- Klinck, J. M., E. E. Hofmann, R. C. Beardsley, B. Salihoglu, and S. Howard (2004), Water-mass properties and circulation on the west Antarctic Peninsula Continental Shelf in Austral Fall and Winter 2001, *Deep Sea Research Part II:*

Topical Studies in Oceanography, 51, 1925–1946,
doi:10.1016/j.dsr2.2004.08.001.

Kohut, J., T. Miles, K. Bernard, W. Fraser, D. Patterson-Fraser, M. Oliver, M. Cimino, P. Winsor, H. Statscewich, and E. Fredj (2016), Project CONVERGE: Impacts of local oceanographic processes on Adélie penguin foraging ecology, pp. 1–7, IEEE.

Lavoie, D., Y. Simard, and F. J. Saucier (2000), Aggregation and dispersion of krill at channel heads and shelf edges: the dynamics in the Saguenay-St. Lawrence Marine Park, *Canadian Journal of Fisheries and Aquatic Sciences*, doi:10.1139/f00-138.

Lawson, G. L., P. H. Wiebe, C. J. Ashjian, S. M. Gallager, C. S. Davis, and J. D. Warren (2004), Acoustically-inferred zooplankton distribution in relation to hydrography west of the Antarctic Peninsula, *Deep Sea Research Part II: Topical Studies in Oceanography*, 51(17-19), 2041–2072, doi:10.1016/j.dsr2.2004.07.022.

Mackas, D. L., R. Kieser, and M. Saunders (1997), Aggregation of euphausiids and Pacific hake (*Merluccius productus*) along the outer continental shelf off Vancouver Island, ... *Journal of Fisheries ...*, doi:10.1139/f97-113.

Martinson, D. G. (2012), Antarctic circumpolar current's role in the Antarctic ice system: An overview, *Palaeogeography, Palaeoclimatology, Palaeoecology*, 335-336, 71–74, doi:10.1016/j.palaeo.2011.04.007.

Martinson, D. G., and D. C. McKee (2012), Transport of warm Upper Circumpolar Deep Water onto the western Antarctic Peninsula continental shelf, *Ocean Science Discussions*, 8, 433–442, doi:10.5194/os-8-433-2012.

Martinson, D. G., S. E. Stammerjohn, R. A. Iannuzzi, R. C. Smith, and M. Vernet (2008), Western Antarctic Peninsula physical oceanography and spatio-temporal variability, *Deep Sea Research Part II: Topical Studies in Oceanography*, 55(18-19), 1964–1987, doi:10.1016/j.dsr2.2008.04.038.

Matano, R. P., A. L. Gordon, R. D. Muench, and E. D. Palma (2002), A numerical study of the circulation in the northwestern Weddell Sea, *Deep Sea Research Part II: Topical Studies in Oceanography*, 49(21), 4827–4841.

Meredith, M. P., and J. C. King (2005), Rapid climate change in the ocean west of the Antarctic Peninsula during the second half of the 20th century, *Geophysical Research Letters*, 32(19), L19604, doi:10.1029/2005GL024042.

Meredith, M. P., S. E. Stammerjohn, H. J. Venables, H. Ducklow, D. G. Martinson, R. A. Iannuzzi, M. J. Leng, J. M. van Wessem, C. H. Reijmer, and N. E. Barrand (2017), Changing distributions of sea ice melt and meteoric water west of the Antarctic Peninsula, *Deep Sea Research Part II: Topical Studies in Oceanography*, 139, 40–

57, doi:10.1016/j.dsr2.2016.04.019.

Moffat, C., B. Owens, and R. C. Beardsley (2009), On the characteristics of Circumpolar Deep Water intrusions to the west Antarctic Peninsula Continental Shelf, *Journal of Geophysical Research*, 114, C05017, doi:10.1029/2008JC004955.

Moffat, C., R. C. Beardsley, and B. Owens (2008), A first description of the Antarctic Peninsula Coastal Current, *Deep Sea Research II*, 55, 277–293, doi:10.1016/j.dsr2.2007.10.003.

Montes-Hugo, M., S. C. Doney, H. Ducklow, W. Fraser, D. G. Martinson, S. E. Stammerjohn, and O. Schofield (2009), Recent changes in phytoplankton communities associated with rapid regional climate change along the western Antarctic Peninsula, *Science*, 323(5920), 1470–1473, doi:10.1126/science.1164533.

Oliver, M. J., A. Irwin, M. A. Moline, W. Fraser, D. Patterson, O. Schofield, and J. Kohut (2013), Adélie Penguin Foraging Location Predicted by Tidal Regime Switching, edited by D. Hyrenbach, *PLoS ONE*, 8(1), e55163, doi:10.1371/journal.pone.0055163.

Oreiro, F. A., E. D'Onofrio, W. Grismeyer, M. N. Fiore, and M. N. Saraceno (2014), Comparison of tide model outputs for the northern region of the Antarctic Peninsula using satellite altimeters and tide gauge data, *Polar Science*, 8(1), 10–23, doi:10.1016/j.polar.2013.12.001.

Orsi, A. H., T. Whitworth, and W. D. Nowlin (1995), On the meridional extent and fronts of the Antarctic Circumpolar Current, *Deep-Sea Research Part I*.

Pelland, N. A., C. C. Eriksen, and C. M. Lee (2013), Subthermocline Eddies over the Washington Continental Slope as Observed by Seagliders, 2003–09, *Journal of Physical Oceanography*, 43, 2025–2053, doi:10.1175/JPO-D-12-086.1.

Piñones, A., E. E. Hofmann, M. S. Dinniman, and J. M. Klinck (2011), Lagrangian simulation of transport pathways and residence times along the western Antarctic Peninsula, *Deep Sea Research II*, 58(13-16), 1524–1539, doi:10.1016/j.dsr2.2010.07.001.

Powers, J. G. et al. (2003), Real-Time Mesoscale Modeling Over Antarctica: The Antarctic Mesoscale Prediction System*, <http://dx.doi.org/10.1175/BAMS-84-11-1533>, 84(11), 1533–1545, doi:10.1175/BAMS-84-11-1533.

Prandtl, L. (1925), *Bericht über Untersuchungen zur ausgebildeten Turbulenz*, Zeitschrift für angewandte Mathematik und Mechanik.

Prézelin, B. B., E. E. Hofmann, C. Mengelt, and J. M. Klinck (2000), The linkage between Upper Circumpolar Deep Water (UCDW) and phytoplankton

- assemblages on the west Antarctic Peninsula continental shelf, *Journal of Marine Research*, 58, 165–202.
- Prézelin, B. B., E. E. Hofmann, M. Moline, and J. M. Klinck (2004), Physical forcing of phytoplankton community structure and primary production in continental shelf waters of the Western Antarctic Peninsula, *J. Mar. Res.*, Vol. 3 (1948), pp. 276–295, 62(3), 419–460, doi:10.1357/0022240041446173.
- Pritchard, H. D., S. R. M. Ligtenberg, H. A. Fricker, D. G. Vaughan, M. R. van den Broeke, and L. Padman (2012), Antarctic ice-sheet loss driven by basal melting of ice shelves, *Nature*, 484, 502–505, doi:10.1038/nature10968.
- Rignot, E., and S. S. Jacobs (2002), Rapid Bottom Melting Widespread near Antarctic Ice Sheet Grounding Lines, *Science*, 296(5575), 2020–2023, doi:10.1126/science.1070942.
- Rignot, E., J. Mouginot, M. Morlighem, H. Seroussi, and B. Scheuchi (2014), Widespread, rapid grounding line retreat of Pine Island, Thwaites, Smith, and Kohler glaciers, West Antarctica, from 1992 to 2011, *Geophysical Research Letters*, 41(5), 3502–3509, doi:10.1029/2011GL046583.
- Rignot, E., S. Jacobs, J. Mouginot, and B. Scheuchl (2013), Ice-shelf melting around Antarctica, *Science*, 341(6143), 266–270, doi:10.1126/science.1235798.
- Savidge, D. K., and J. A. Amft (2009), Circulation on the West Antarctic Peninsula derived from 6 years of shipboard ADCP transects, *Deep-Sea Research Part I*, 56(10), 1633–1655, doi:10.1016/j.dsr.2009.05.011.
- Schmidtko, S., K. J. Heywood, A. F. Thompson, and S. Aoki (2014), Multidecadal warming of Antarctic waters, *Science*, 346, 1227–1231, doi:10.1126/science.1256117.
- Schofield, O. et al. (2007), Slocum Gliders: Robust and ready, *Journal of Field Robotics*, 24(6), 473–485, doi:10.1002/rob.20200.
- Schofield, O. et al. (2013), Penguin Biogeography Along the West Antarctic Peninsula: Testing the Canyon Hypothesis with Palmer LTER Observations, *Oceanography*, 26(3), 204–206, doi:10.5670/oceanog.2013.63.
- Schofield, O. et al. (2017a), Decadal variability in coastal phytoplankton community composition in a changing West Antarctic Peninsula, *Deep-Sea Research Part I*, 124, 42–54, doi:10.1016/j.dsr.2017.04.014.
- Schofield, O. et al. (2017b), Decadal variability in coastal phytoplankton community composition in a changing West Antarctic Peninsula, *Deep-Sea Research Part I*, doi:10.1016/j.dsr.2017.04.014.

- Sievers, H. A., and W. D. Nowlin (1984), The stratification and water masses at Drake Passage, *Journal of Geophysical Research: Oceans*, 89(C6), 10489–10514, doi:10.1029/JC089iC06p10489.
- Smith, D. A., and J. M. Klinck (2002), Water properties on the west Antarctic Peninsula continental shelf: a model study of effects of surface fluxes and sea ice, *Deep Sea Research Part II: Topical Studies in Oceanography*, 49, 4863–4886, doi:10.1016/S0967-0645(02)00163-7.
- Smith, D. A., C. M. Lascara, J. M. Klinck, and E. E. Hofmann (1995a), Palmer LTER: Hydrography in the inner shelf region, *Antarctic Journal of the United States*, 30, 258–260.
- Smith, D. A., E. E. Hofmann, J. M. Klinck, and C. M. Lascara (1999), Hydrography and circulation of the West Antarctic Peninsula Continental Shelf, *Deep-Sea Research Part I*, 46, 925–949.
- Smith, R. C. et al. (1995b), The Palmer LTER: A long-term ecological research program at Palmer Station, Antarctica, *Oceanography*, 8, 77–86.
- St-Laurent, P., J. M. Klinck, and M. S. Dinniman (2013), On the Role of Coastal Troughs in the Circulation of Warm Circumpolar Deep Water on Antarctic shelves, *Journal of Physical Oceanography*, 43, 51–64, doi:10.1175/JPO-D-11-0237.1.
- Stammerjohn, S. E., and R. C. Smith (1996), *Spatial and Temporal Variability of Western Antarctic Peninsula Sea Ice Coverage*, Antarctic Research Series, American Geophysical Union, Washington, D. C.
- Stammerjohn, S. E., D. G. Martinson, R. C. Smith, and R. A. Iannuzzi (2008a), Sea ice in the western Antarctic Peninsula region: Spatio-temporal variability from ecological and climate change perspectives, *Deep Sea Research ...*, 55(18-19), 2041–2058, doi:10.1016/j.dsr2.2008.04.026.
- Stammerjohn, S. E., D. G. Martinson, R. C. Smith, X. Yuan, and D. Rind (2008b), Trends in Antarctic annual sea ice retreat and advance and their relation to El Niño–Southern Oscillation and Southern Annular Mode variability, *Journal of Geophysical Research: Oceans*, 113(C3), C03S90, doi:10.1029/2007JC004269.
- Thoma, M., A. Jenkins, D. Holland, and S. Jacobs (2008), Modelling Circumpolar Deep Water intrusions on the Amundsen Sea continental shelf, Antarctica, *Geophysical Research Letters*, 35(18), 3223, doi:10.1029/2008GL034939.
- Thompson, D. W. J., and S. Solomon (2002), Interpretation of Recent Southern Hemisphere Climate Change, *Science*, 296(5569), 895–899, doi:10.1126/science.1069270.

- Turner, J., H. Lu, I. White, J. C. King, T. Phillips, J. S. Hosking, T. J. Bracegirdle, G. J. Marshall, R. Mulvaney, and P. Deb (2016), Absence of 21st century warming on Antarctic Peninsula consistent with natural variability, *Nature*, 535(7612), 411–415, doi:10.1038/nature18645.
- Turner, J., T. A. Lachlan-Cope, S. Colwell, G. J. Marshall, and W. M. Connolley (2006), Significant Warming of the Antarctic Winter Troposphere, *Science*, 311, 1914–1917, doi:10.1126/science.1121652.
- Turner, J., T. Maksym, T. Phillips, G. J. Marshall, and M. P. Meredith (2012), The impact of changes in sea ice advance on the large winter warming on the western Antarctic Peninsula, *Int. J. Climatol.*, 33(4), 852–861, doi:10.1002/joc.3474.
- Vaughan, D. G. (2005), How Does the Antarctic Ice Sheet Affect Sea Level Rise? *Science*, 308(5730), 1877–1878, doi:10.2307/3841440.
- Venables, H. J., M. P. Meredith, and J. A. Brearley (2016), Modification of deep waters in Marguerite Bay, western Antarctic Peninsula, caused by topographic overflows, *Deep Sea Research Part II: Topical Studies in Oceanography*, doi:10.1016/j.dsr2.2016.09.005.
- von Storch, H., and F. W. Zwiers (1999), *Statistical Analysis in Climate Research*, Cambridge University Press, Cambridge, UK.
- Wallace, M. I., M. P. Meredith, M. A. Brandon, T. J. Sherwin, A. Dale, and A. Clarke (2008), On the characteristics of internal tides and coastal upwelling behaviour in Marguerite Bay, west Antarctic Peninsula, *Deep Sea Research Part II: Topical Studies in Oceanography*, 55(18-19), 2023–2040, doi:10.1016/j.dsr2.2008.04.033.
- Zhou, M., Y. Zhu, and J. O. Peterson (2004), In situ growth and mortality of mesozooplankton during the austral fall and winter in Marguerite Bay and its vicinity, *Deep Sea Research Part II: Topical Studies in Oceanography*, 51(17-19), 2099–2118, doi:10.1016/j.dsr2.2004.07.008.